



Fluid inclusion studies of the Kenticha rare-element granite-pegmatite, Southern Ethiopia

Barsisa Bekele^{1,2} · Amit Kumar Sen¹

Received: 4 February 2022 / Revised: 24 June 2022 / Accepted: 28 June 2022 / Published online: 27 July 2022

© The Author(s), under exclusive licence to Science Press and Institute of Geochemistry, CAS and Springer-Verlag GmbH Germany, part of Springer Nature 2022

Abstract In the Kenticha area, a series of barren to rare metal-bearing pegmatites intruded into the Neoproterozoic Adola Belt. The pegmatites host world-class Nb and Ta deposits and significant Li and Be reserves. In this contribution, fluid inclusion data and feldspar geothermometry have been combined to define the crystallization condition of the Kenticha rare-metal pegmatite. Primary and complex assemblages of secondary fluid inclusions representing episodic fluid circulations have been identified in quartz and spodumene. A primary aqueous-carbonic fluid of low salinity aqueous solution with liquid and vapour CO₂ phases, secondary carbonic fluid rich and carbonic-only fluids, and multiple generations of secondary aqueous inclusions that represent sub-solidus hydrothermal circulation have been identified. All aqueous inclusions were homogenized into the liquid phase between 100 and 290 °C. Aqueous-carbonic inclusions were homogenized, usually via a critical transition [$T_h(LV \rightarrow SCF)$] between 241 and 397 °C, or less commonly, via a dew-point transition [$T_h(LV \rightarrow V)$] between 213 and 264 °C. Crystallization of the rare-element pegmatite is certainly associated with the late-stage magmatic or early hydrothermal low-salinity aqueous-carbonic fluid that homogenizes to critical conditions. A combination of

microthermometric data and existing experimentally determined solidus from flux and volatile bearing haplogranite suggests exsolution of fluids from hydrous silicate melt, perhaps during crystallization of the aplitic layer. The fluids were then trapped and isobarically cooled along a reasonable geothermal gradient within the pegmatite unit down to a temperature of around 397 °C.

Keywords Fluid inclusions · Microthermometry · Pegmatite · Cooling-path · Boiling · Kenticha

1 Introduction

Pegmatite has received considerable interest over the past decades because it is the primary source of strategic rare metals, ceramic and glass materials, and various gemstones. In particular, evolved pegmatites are a source of a wide variety of rare metals such as Li, Rb, Cs, Sn, Ta, Nb, and Sc so far (Černý 1991), that would crystallize as exotic minerals. The occurrences of exotic minerals and mineralogical and textural zonation in the more evolved peraluminous granitic pegmatites are the effects of non-equilibrium fractional crystallization and/or due to the complex interplay of volatiles and fluxing agents in the melt (London 1986; London and Kontak 2012; London and Morgan 2012; Wood and Williams-Jones, 1993). During the course of silicate melt evolution, the volatile and fluxing components “scour” the incompatible rare elements from the deeper part of the magma, and incorporate them into late-stage crystallized phases or form exotic minerals at shallow depths (Jahns and Burnham 1969). Based on experimental studies on simple silicate-H₂O systems, petrologists surmise that the rare-element bearing

✉ Barsisa Bekele
bakoket2@gmail.com

Amit Kumar Sen
senakfes@gmail.com; amit.sen@es.iitr.ac.in

¹ Department of Earth Sciences, Indian Institute of Technology Roorkee, Roorkee, India

² Department of Earth Sciences, Wollega University, Nekemte, Ethiopia

pegmatites are most likely to crystallize from a very silicic residual melt enriched with rare and rare-alkali elements (e.g., Li, Rb, Cs, Be, Sr, and Ba), flux (e.g., B, F, and P), and volatile (e.g., H₂O, Cl) components (London, 1986; London and Kontak, 2012). The presence of volatiles and fluxing components would control melt properties by lowering viscosity and decreasing solidus and liquidus temperatures (e.g., London 1986; London and Morgan 2012). They also decrease nucleation rates but increase diffusion rates and solubility, which ultimately favour crystal growth and enrichment of lithophile elements and rare metals in the remaining melt.

The fluid inclusions contained in pegmatites are directly derived from cooling silicate melt, trapped from metamorphic fluid, or post-crystallization hydrothermal fluid circulations (Anderson et al. 2001). These inclusions are useful in appraising the fluid process and thermal history of granitic pegmatites (Beurlen et al. 2000; Cameron et al. 1953; Fuertes-fuente et al. 2000; Nabelek and Ternes 1997; Roedder 1963; Shelton and Orville 1980; Shepherd et al. 1985; Whitworth and Rankin 1989). According to these studies, a wide range of fluid inclusion compositions and pressure–temperature (P–T) conditions for the last stage of pegmatite crystallization were reported. Studies independently conducted by London (1986); Trumbull (1995); and Whitworth and Rankin (1989) have shed light on fluid inclusion application in reconstructing the crystallization conditions of rare-element pegmatites. By integrating thermometric data and lithium aluminosilicate phase relationships, they have outlined the P–T path of pegmatite crystallization from different parts of the world.

The Kenticha rare element pegmatite hosts world-class deposits of Ta and Nb and remarkable reserves of Li and Be (Kozyrev et al. 1982). The pegmatites' mineralization, geochemistry, and mineralogy are well documented (Bekele and Sen 2020; Küster 2009; Solomon and Zerihun 1996; Tadesse 2001). However, the cooling path and the physicochemical conditions of the rare-metal pegmatite are yet to be carried out. Therefore, this paper aims to present the outcome of *PVTX* properties of fluid inclusions studies and indicate the cooling path and crystallization conditions of the Kenticha rare element pegmatite. This study integrated microthermometric data, lithium aluminosilicate phase relationships, and an independent estimate of the temperature of the last-stage crystallization conditions of the rare metal pegmatite based on a two-feldspar geothermometer. For the latter case, the assumption is that the compositions of coexisting feldspar pairs are dictated solely by the pressure and temperature conditions, provided that the two feldspars attain complete stable equilibrium (Benisek et al. 2004).

2 Geological setting

This study pertains to the Kenticha rare-element granite-pegmatite situated in the Neoproterozoic Adola belt of southern Ethiopia. The Adola Neoproterozoic lithotectonic terranes occupy a transitional position between the south of the juvenile crust of the Arabian Nubian Shield (ANS) and the north of the lower crustal Pan-African Mozambique belt (MB) (Bisrat et al. 2003, 2002; Küster 2009; Stern et al. 2012). In the Adola belt, the volcano-sedimentary and associated mafic–ultramafic rocks are juxtaposed to the high-grade gneisses of the Mozambique belt along the N–S striking thrust and shear zones (Allen and Tadesse 2003; Beraki et al. 1989; Bisrat et al. 2002; Fritz et al. 2013; Hailu and Schandelmeier 1996; Stern and Dawoud 1991). The southern Ethiopian crystalline rocks were essentially developed due to plate collision and lithospheric thickening which is substantiated by the presence of the fold and thrust belts and granulite facies rocks (Tsige 2006 and reference therein). The N–S striking thrust and shear zones, which separate each lithotectonic unit, were developed between 680 and 630 Ma through repeatedly reactivated deformations (Allen and Tadesse 2003; Beraki et al. 1989; Hailu and Schandelmeier 1996; Küster 2009) (Fig. 1). Within the Adola Neoproterozoic shear belt, the narrow N–S trending syncline, predominantly of juvenile Neoproterozoic supracrustal and magmatic assemblages, was regarded as the Kenticha ultramafic belt (Beraki et al. 1989; Hailu and Schandelmeier 1996). Hailu and Schandelmeier (1996) have interpreted structural and geochemical data on rocks affiliated with the Neoproterozoic Adola belt as a typical Wilson Cycle process. They further indicated that the Kenticha terrane is assumed to have been developed during the initial stage of these processes, i.e., the evolution of a passive continental margin and ocean floor formation. It is underpinned by the presence of metamorphosed passive continental margin psammo-pelitic sediments and associated ultrabasic suites within the Kenticha greenstone belts (Hailu and Schandelmeier 1996). This phase was followed by subsequent subduction and arc development in the Megado terrane, which followed the closure of the ocean basin.

The Kenticha pegmatite field represents the largest rare-metal pegmatite field currently known in the Horn of Africa (Tadesse 2001) that intruded into the Kenticha greenstone belts. These pegmatites are genetically and temporally linked to the post-orogenic granite intrusions that appear to be emplaced in ultramafic rock nearly along the NE–SW trending dilation zone of the major regional fault (Figs. 1 and 2) and sets of fractures (Küster et al. 2009; Zerihun et al. 1995) around 550–520 Ma (Hailu and Schandelmeier 1996). These genetically linked granites

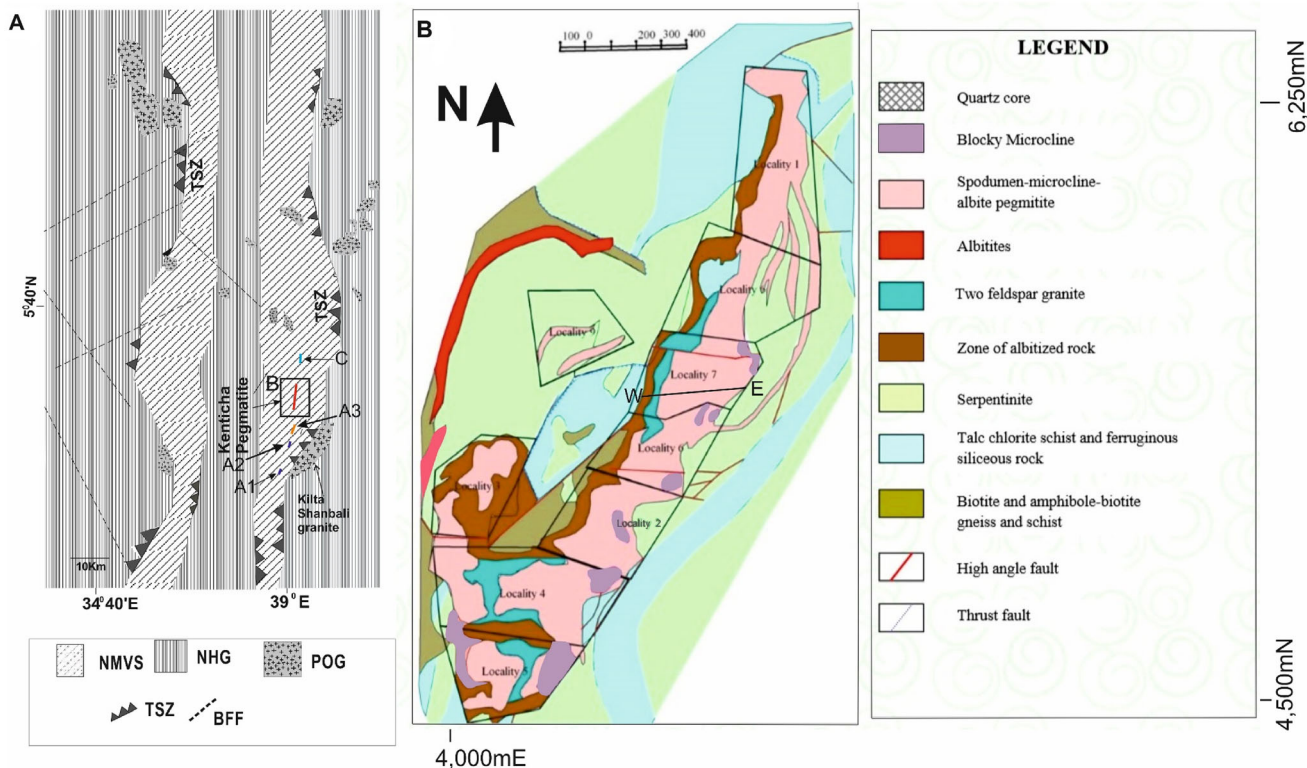


Fig. 1 Geological map of **A.** Adola Belt after Hailu and Schandelmeier (1996), **B.** Kenticha rare element granite–pegmatite main body after Ethiopian Mineral, Petroleum and Biofuel Corporation (EMPBC). *NMVS.* Neoproterozoic metavolcanic rocks, *MPOC.* Mesoproterozoic & older crust, *POG.* post-orogenic granite, *TSZ.* thrust and shear zone, *BFF.* brittle fold and fault, *AA.* Addis Ababa, *A1.* Dermi Dama pegmatites, *A2.* Kilkille pegmatites *A3.* Shuni Hill pegmatites, *C.* Bupho pegmatite

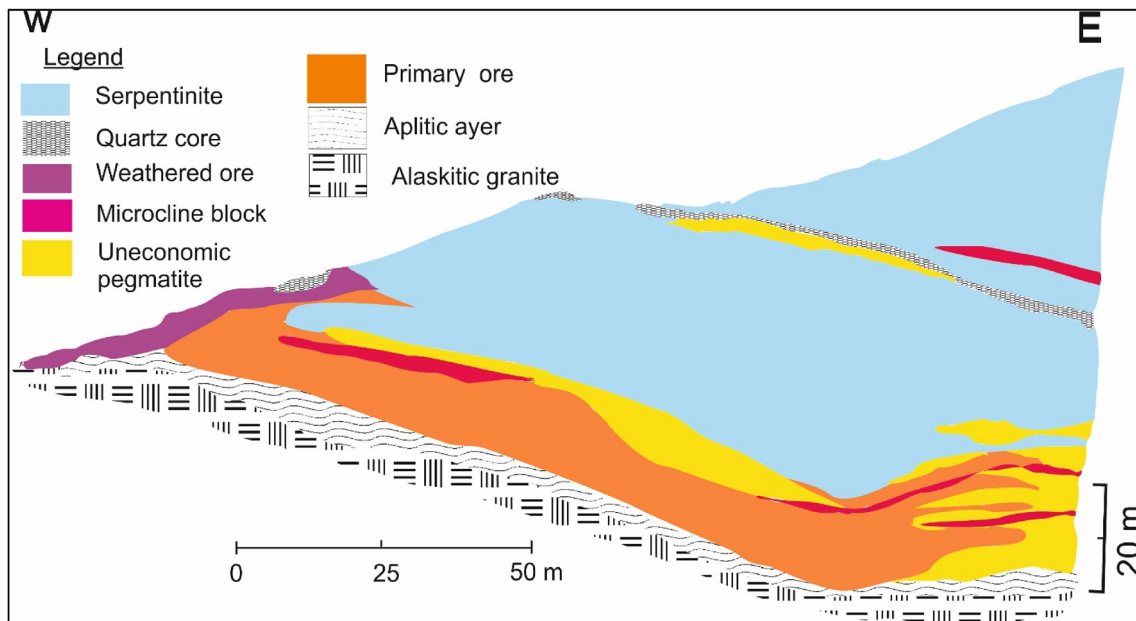


Fig. 2 Cross-section of the Kenticha rare element granite–pegmatite (locality 7, Fig. 1B)

have been identified as alaskitic granite, biotite granite, and two-mica granite (cf. Solomon and Zarihun 1996). The main Kenticha rare-element granite-pegmatite body and

associated satellite pegmatites are cropping out extensively in the NW flank of the two-mica granite batholith. With increasing distance away from the two-mica granite, the

pegmatites show typical regional fractionation trends varying from proximal barren (see A1, Fig. 1) to distal albite-spodumene types (C) (Küster et al. 2009; Solomon and Zerihun 1996; Tadesse 2001). The beryl-columbite types (A2 and A3) and complex spodumene-type pegmatites (B) are present between the two extreme pegmatite ends.

2.1 Kenticha rare-element pegmatite mineralogy

The Kenticha rare-element granite-pegmatite is texturally zoned and mineralogically graded from bottom to top (Küster et al. 2009). The conventional terminology used to denote different units of concentrically zoned pegmatite, i.e., “border zone,” “wall zone,” “intermediate zone,” and “core zone,” has been replaced by “lower zone,” “intermediate zone,” and “upper zone” for simplicity and, most importantly, due to the vertical zonation and sub-horizontal shape of the Kenticha rare element granite-pegmatite (Küster et al. 2009) (Fig. 2). The *lower zone* essentially consists of medium-grained quartz, albite, alkali-feldspar, and muscovite in the alaskitic granite, and albite and quartz in the aplitic granite (Fig. 3A). However, in both alaskitic granite and the aplitic layer, albite is dominant over K-feldspar. The *intermediate zone* is represented by muscovite-quartz-albite-microcline pegmatite. The minerals present in the intermediate pegmatite unit (Fig. 3B) are muscovite, quartz, microcline, and albite in its lower portion. Accessory minerals in this unit include pyrite, ilmenite, arsenopyrite, and magnetite. The upper part of the intermediate zone is dominated by quartz, spodumene, and microcline. The presence of lithian muscovite, lepidolite, mixed-form, green muscovite, secondary biotite, and sericite was evident in the intermediate and upper zones. The *upper (core) zone* is characterized by a discontinuously developed quartz unit, a continuous radial spodumene unit, discontinuous lenses of blocky microcline unit, and a saccharoidal albite unit. The saccharoidal albite is found mainly in the lower margin of the upper zone. Lath-shaped albite, coarse radial aggregates of albite (cleavelandite), and fine-grained saccharoidal albite are widespread. The highly albitized zone of the pegmatite is generally rich in columbite-tantalite crystals. Multiple *microcline blocks* have discontinuously occurred in the upper zone parallel to the contacts of the pegmatite body. They frequently form separate veins within the pegmatite body and also occur intergrown with quartz or plagioclase. *Spodumene unit* is continuously formed in the upper unit. The unit is mineralogically characterized by a muscovite–quartz–albite–microcline–spodumene assemblage. It forms a lath-shaped or occasionally a box-work structure around quartz or albite. The *quartz core* is discontinuously developed as big lenses and massive boulders that locally form blocks of up

to 30 m². The ore minerals of Ta-Nb, Be, and Li show progressive enrichment towards the pegmatite core (upper) zone. The ore deposit of rare metals occurs in three forms: alluvial and diluvial placer ores; the lateritic type ore, and the primary ore.

Generally, quartz is a principal constituent throughout the pegmatite body, which varies considerably in size and shape. Quartz often occurs intergrown with other minerals (spodumene, feldspar). The feldspar group minerals are substantial components in the granite-pegmatite, which locally attains up to 70% by volume. Albite, orthoclase, and microcline are the dominant feldspar group minerals, with subordinate amazonite and anorthoclase. White mica is found throughout the pegmatite zone, with the average percentage estimated to be 4–16% by volume. Muscovite is the dominant white mica in the Kenticha pegmatite. Spodumene (α -LiAlSi₂O₆), (Fig. 3C), is a primary lithium aluminosilicate phase present and constitutes 5 to 45 modal % of the rare metal pegmatite. Petalite is associated with coarse-grained potassic feldspar and quartz, indicating primary origins that crystallize directly from the cooling silicate melt (Brown and Parsons, 1981). The presence of other forms of primary lithium aluminosilicate phases was not confirmed during the present study. The metastability of petalite in the near-surface environment is attributed to the solubility of aluminosilicate minerals being enhanced by the presence of late-stage subsolvus CO₂-rich fluids (London et al. 1982a).

Texturally, the pegmatite is bimodal, particularly in the spodumene unit. It comprises large quartz, spodumene, and feldspar grains filled in a saccharoidal albite-quartz matrix. Intergrowths of quartz and spodumene (squi) and blebs of plagioclase hosted by alkali-feldspars (perthite) are frequently encountered in intermediate to upper pegmatite units. Occasionally, muscovite and lepidolite are enclosed poikilitically within the quartz. The majority of alkali-feldspars from pegmatite are turbid and have coarse exsolution microtextures. Graphic intergrowth, overgrowth (plagioclase on alkali-feldspar), and aplitic texture occur in the lower zone. Intergrowths of quartz and sporadic blocks of alkali-feldspar occur in aplite, which grades into the lower intermediate zone by increasing the size of the blocky alkali-feldspar with/without intergrowth with quartz. Generally, the pegmatite main ore body shows an increase in quartz–alkali feldspar/spodumene intergrowths from the lower to the upper zone.

3 Sample and analytical methods

Representative rock and mineral samples were collected from the rare-metal granite-pegmatite and the surrounding barren pegmatite. Wafers of quartz and spodumene

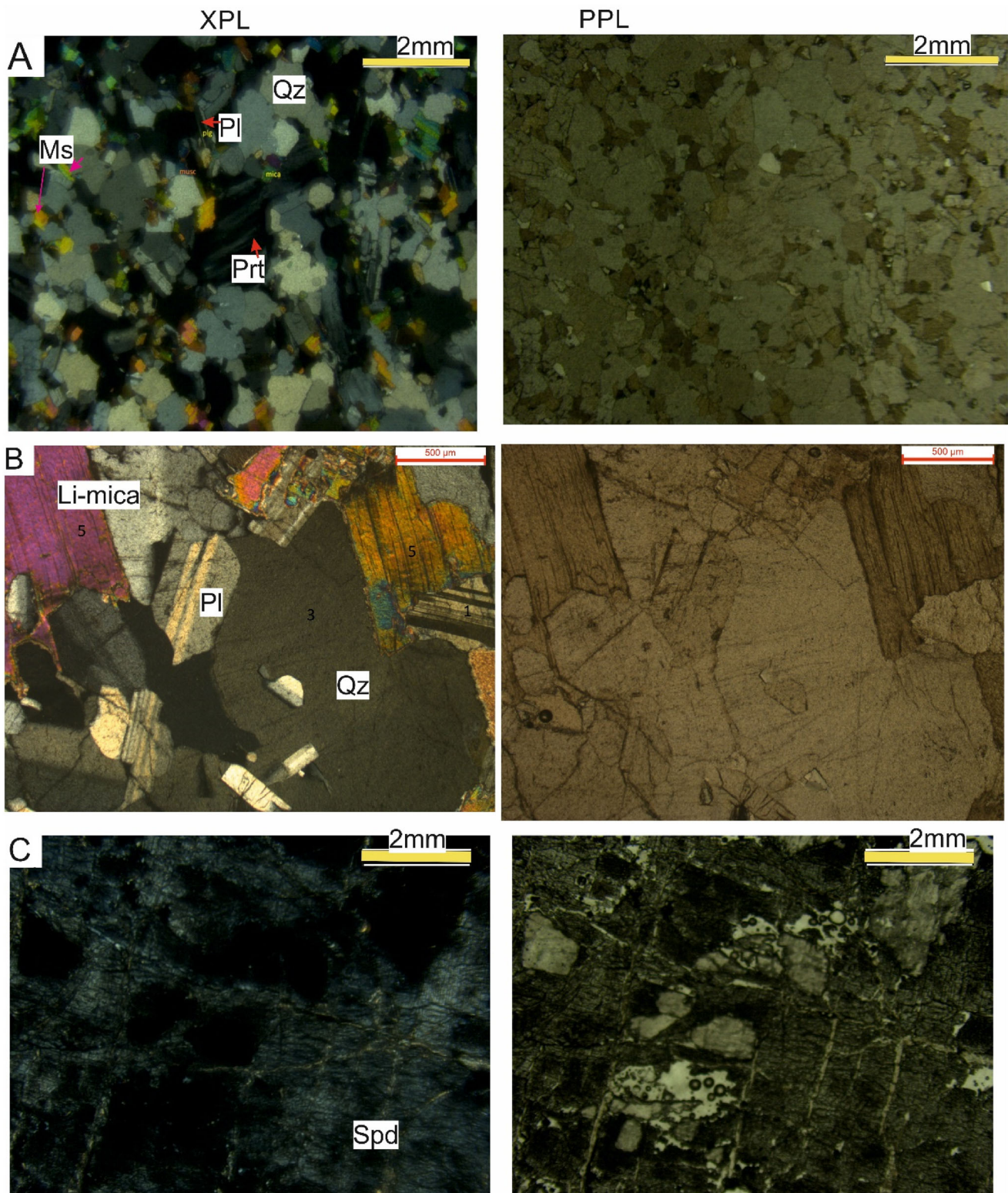


Fig. 3 Photomicrographs of **A.** granite unit, **B.** intermediate pegmatite, and **C.** spodumene sample. Left images are taken under XPL – cross-polarized light and the right images are in PPL – plane-polarized light. Spd – spodumene, Li-mica–lithium mica, Qz. quartz, prt. perthite, Pl. plagioclase

samples were prepared and studied under a transmitted light microscope to provide the fluid inclusions' petrographic and paragenetic framework. A summary of the textural and spatial relationships between fluid inclusions has been sketched. Quartz specimens were chosen for microthermometric analysis due to the presence of abundant and relatively large inclusions, the inertness of quartz to trapped fluids, and its low thermal expansion. The degree of fill was estimated at room temperature except for non-aqueous inclusions. For the latter, it was recorded at a fairly lower temperature than the room temperature but higher than the final clathrate melting temperature. For microthermometric analysis, we selected appropriate inclusion sizes from all types of fluid inclusions.

Microthermometric studies of fluid inclusions were carried out using the LINKAM THMSG 600 heating-freezing stage fitted on a Nikon LV 100 Pol microscope in the Ore Geology Laboratory, Department of Earth Sciences, Indian Institute of Technology Roorkee (IIT Roorkee). Sufficiently large inclusions in the range of 15 to 30 μm have been selected for microthermometric studies. During the heating-freezing cycle, phase changes and the temperature at which they occur have been recorded. Cooling was routinely achieved at a temperature of $-120\text{ }^\circ\text{C}$. During subsequent warming of frozen inclusions, the temperatures of the first appearance of liquid (eutectic, T_e), the final disappearance of ice [$T_m(\text{ice})$], the melting temperature of solid CO_2 [$T_m(\text{CO}_2)$], the clathrate melting temperature [$T_m(\text{Cla})$], partial homogenization temperature of CO_2 [$T_h(\text{CO}_2)$], total homogenization temperature [$T_h(\text{LV})$], and temperature of decrepitation of inclusions (T_d) were recorded. The $T_h(\text{LV})$ and $T_m(\text{ice})$ were reproduced at a temperature of $\pm 3\text{--}6\text{ }^\circ\text{C}$, whereas $T_m(\text{CO}_2)$ and $T_m(\text{Cla})$ were reproduced at a temperature of $\pm 0.5\text{--}1.0\text{ }^\circ\text{C}$. The LINKAM THMSG 600 heating-freezing stage can be cooled to -196 and heated to $+600\text{ }^\circ\text{C}$. The stage was calibrated using a triple point of pure CO_2 ($-56.6\text{ }^\circ\text{C}$) and H_2O with a homogenization temperature of $374.1\text{ }^\circ\text{C}$ via critical phenomenon. Repeated heating and freezing cycles were carried out near the anticipated $T_m(\text{Cla})$ and $T_h(\text{LV})$ to get accurate results, as suggested by Shepherd et al. (1985). When measuring $T_m(\text{CO}_2)$, $T_h(\text{CO}_2)$, $T_m(\text{ice})$, and $T_m(\text{Cla})$, a heating rate of $0.5\text{--}5\text{ }^\circ\text{C}/\text{min}$ was used, whereas $T_h(\text{LV})$ was measured at a rate of $3\text{--}5\text{ }^\circ\text{C}/\text{min}$. The minimum heating rate was taken at the incipient phase change. In this paper, the terms “carbonic” and “eutectic” represent the mixture of liquid or gaseous CO_2 , CH_4 , and N_2 , and the first melting temperature of ice, respectively. We visually estimated the volumetric proportions of fluid inclusion phases based on the Bakker and Diamond (2006) chart. Symbols and terms are based on the explanation presented in Diamond (2003). The compositions of the feldspar pairs were analysed using a CAMECA SX100 Electron Probe

Micro-Analyser (EPMA) at the Institute Instrumentation Centre, IIT Roorkee. Measurement was performed using jadeite ($\text{NaK}\alpha$), wollastonite ($\text{CaK}\alpha$) and orthoclase ($\text{AlK}\alpha$, $\text{SiK}\alpha$, $\text{KK}\alpha$) calibration standards. An online ZAF correction procedure was applied to the EPMA data. Measurements were performed at the instrumental conditions of a 15 keV accelerating voltage and a 20 nA electron beam current focused on a $1\text{ }\mu\text{m}$ spot size. Signal counting times were 20 s on peak and 10 s on each side. The detection limits above the mean background were 0.02 wt%. Si, Al, Mg, and Na analyses were conducted on the TAP crystal; Ca, K, and Ti on the PETJ crystal, whereas Fe and Mn were analysed on the LIFH crystal. The data was processed with an online ZAF correction procedure using the PAP algorithm (Pouchou and Pichoir 1991). Averages of eight-spot analyses per grain were taken.

4 Results

4.1 Fluid inclusion's petrography

The fluid inclusions have been classified and distinguished based on shape, phases, volumetric proportions, distribution with respect to crystallographic elements, and secondary features of the host mineral based on the criteria presented in Roedder (1984) and Shepherd et al. (1985). Petrographic observations reveal the presence of ubiquitous fluid inclusions hosted in quartz and spodumene specimens. However, more abundant and prominent inclusions are found in the former mineral specimens. In spodumene, the primary fluid inclusions commonly occur as sub-rounded and negative crystal shapes with an average diameter in the range of up to 5 to 20 μm . In quartz, large-sized primary inclusions (up to 30 μm), as well as numerous trails of different generations of pseudo-secondary and secondary fluid inclusions, which occasionally cross-cut one another along crystallographic planes or healed microfractures, are present. Primary fluid inclusions are distributed in clusters, locally isolated, and relatively less abundant. They occur in crystallographic planes or growth zones, whereas secondary inclusions are abundant, forming trails, and relatively smaller. Comprehensive petrographic studies of the fluid inclusions have been performed on quartz to establish paragenetic sequences and trace fluid evolution (Fig. 4). Accordingly, three episodes of fluid circulation that were trapped during or post-crystallization of the pegmatites are recorded in quartz. (1) Isolated individuals, clustered inclusions, or randomly distributed inclusions within the host crystal's core. They are primary aqueous-carbonic inclusions (immiscible liquids). Those inclusions that occur parallel to the c-axis occasionally appear as perfectly faceted negative crystal

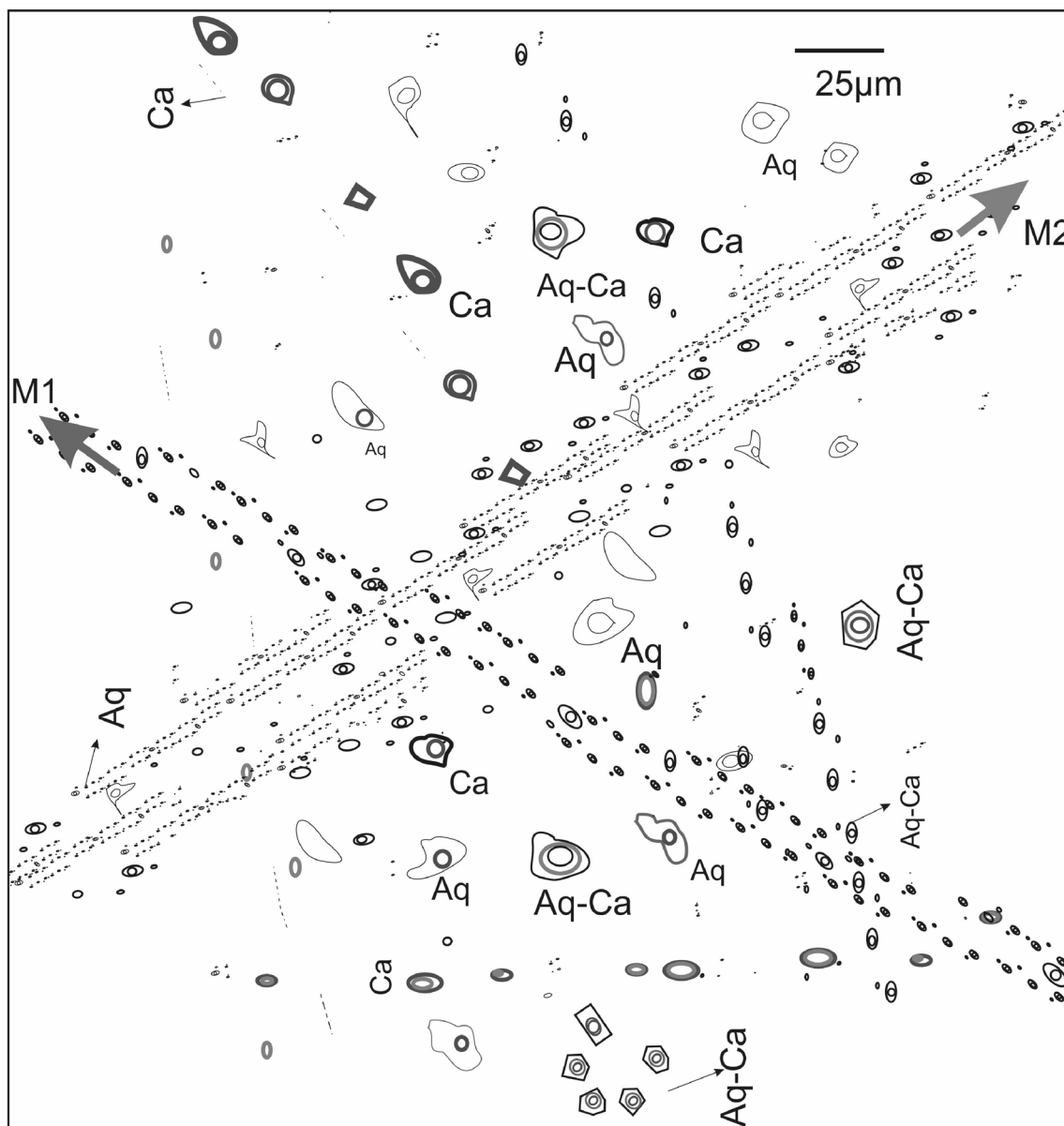


Fig. 4 Schematic diagram showing a summary of fluid inclusion populations entrapped in the different episodes. Aq–Ca: aqueous–carbonic, Aq, aqueous, Ca, carbonic, M1, first generation microfracture, M2, second generation microfracture

shapes. The size of these inclusions is significantly varied and locally reaches up to 30 μm in diameter. This group of inclusions indicates an entrapment in the multiphase field because the composition/density properties and the relative volumetric proportions of the inclusion phases at room temperature are variable. (2) The second stage of fluid entrapment along a first-generation rehealed microfracture (M1) is initiated by mechanical or thermal stress. These inclusions are trapped under conditions of extreme heterogeneity and show a variable aqueous-vapour phase ratio. The inclusions show sporadically irregular, negative crystal shapes and sub-rounded shapes. Necking down is apparent for some inclusions larger than 15 μm . The

inclusions are aligned in microfracture and form trails and represent a fluid inclusion assemblage (FIA). (3) Inclusions trapped in the second-generation microfracture (M2): These inclusions are aligned and elongated parallel to the microfracture that forms trails. This type of inclusion is minimal in distribution and abundance and often undergoes re-equilibration through stretching, necking-down, leakage, or decrepitation. Re-equilibrations appear to be controlled by the size of the inclusions, where large-sized inclusions are commonly affected compared to smaller ones. The inclusions show two contrasting compositions and variable phase ratios, which indicate the rehealing of microfracture and trapping of inclusions over an extended geological

period from two heterogeneous fluids. The entrapment of these fluids is most likely postdating the first-generation fluid. Based on phase content at room temperature, petrographic aspects reveal six inclusion types, in line with the classification scheme of Shepherd et al. (1985). These are (1) liquid phase only, (2) liquid-rich biphasic, (3) vapour phase, (4) vapour-rich biphasic, (5) immiscible liquid, and (6) very rare multiphase solid inclusions. They vary notably in their degree of fill, shape, size, and abundance. Immiscible liquid has been distinguished as the sole primary inclusions identified in quartz and spodumene. Immiscible liquid refers to two or more fluid phases at equilibrium having a contrasting composition (Roedder and Bodnar, 1980) and, in the present paper, represents the ${}^1\text{H}_2\text{O}$ - ${}^1\text{CO}_2$ - ${}^{\text{V}}\text{CO}_2$ fluid system.

4.2 Microthermometry

During freezing-heating, phases including vapour, liquid, solid CO_2 , clathrate, hydrohalite, and solid inclusions have been observed. Microthermometric data of an assemblage of fluid inclusions show slight variation, perhaps attributed to re-equilibration of inclusions, variation in fluid inclusions' shape, and natural fluctuations of temperature and pressure during inclusion entrapment (London et al. 1982; Roedder 1984, 1981, 1963). Based on microthermometric data (Table 1), three main types of fluid inclusions have been identified. These are (1) mixed aqueous-carbonic (${}^{\text{L}}\text{H}_2\text{O}$ - ${}^{\text{L}}\text{CO}_2$ - ${}^{\text{V}}\text{CO}_2$) inclusions approximated by the H_2O - CO_2 - NaCl system and represented as type 1. It includes those inclusions that appear bi-phase at room temperature with no detectable liquid CO_2 . (2) non-aqueous (carbonic) inclusions with a thin layer of or no detectable liquid H_2O , represented as type 2, and (3) aqueous inclusions, approximated by the H_2O - $\text{NaCl} \pm \text{KCl}$ system, and represented by type 3, are another set of inclusions. Microthermometry of monophasic aqueous inclusions was not determined. They are metastable $\text{H}_2\text{O}(\text{L})$ that are thought to be trapped below 70°C (Goldstein and Reynolds, 1994). Photomicrographs of selected fluid inclusions and microthermometric data are shown in Figs. 4 and 5, respectively. The apparent relative darkness of the carbonic inclusions under the optical microscope is a function of the refractive index in the same way as with mineral relief (Fig. 5C). Multiphase solid (L + V + S) inclusions are the rarest of all the types of inclusions studied. The solid phase has a prismatic habit with low birefringence and gets dissolved below total T_{h} .

4.2.1 Mixed aqueous-carbonic inclusions (Type 1)

At room temperature, Type 1 inclusions commonly show three discernible phases (low salinity aqueous liquid, liquid

CO_2 , and gaseous CO_2) when seen under a transmitted light microscope. Some biphasic inclusions gradually developed into three phases during freezing as the vapour bubble nucleated. Type 1 inclusions are commonly seen as large and isolated individuals of $\leq 30\ \mu\text{m}$ in size. Occasionally, these inclusions are clustered, isolated, or locally disseminated. The estimated volume percent of the vapour phase ($V_{\text{g}}/V_{\text{t}} \times 100$) varies from 10 to 60%. The first melting temperature of the carbonic phase and the first ice melting temperature suggest the compositions of these inclusions correspond to an H_2O - CO_2 - NaCl system. However, the presence of small quantities of other volatile components is inevitable since the first melting of the carbonic phase ($T_{\text{m}}\text{CO}_2$) is slightly lower than pure CO_2 eutectic (-56.6°C).

The type 1 primary inclusions show a very narrow range of freezing point depression near the melting temperature of pure CO_2 ($T_{\text{m}}\text{CO}_2 = -56.6$ to -57.1°C), Fig. 6A. The first melting of ice occurs between -15 and -23°C , while the clathrate dissociation [$T_{\text{m}}(\text{Clath})$] occurs between 6.9 and 8.6°C with corresponding salinity of 5.9 to $2.8\ \text{wt}\%$ NaCl equivalent. The partial homogenization temperature [$T_{\text{h}}(-\text{CO}_2)$] ranges between 18 and 30.1°C (Fig. 6B), which commonly occurs in the liquid state. The total homogenization temperatures for inclusions homogenized to the critical phenomenon range from 241 to 397°C , and 213 to 264°C for inclusions homogenized in the vapour state (Fig. 6C). Most commonly, inclusions get homogenized via a critical transition [$T_{\text{h}}(\text{LV} \rightarrow \text{SCF})$], (Fig. 7A), and less commonly, to the vapour state via a dew-point transition [$T_{\text{h}}(\text{LV} \rightarrow \text{V})$]. Some volatile-rich, large inclusions ($> 30\ \mu\text{m}$) were decrepitated (Fig. 7B) between 250 and 275°C upon heating before homogenization temperature was achieved owing to the high internal pressure of the fluids (Roedder and Bodnar, 1980). Aqueous-carbonic inclusions were also seen trapped along cross-cutting first-generation microfractures. These inclusions form trails. The first ice melting temperature occurs between -30 and -35°C , suggesting an H_2O - CO_2 - NaCl - MgO system. We represented this fluid inclusion as type 1b. Its salinity and homogenization temperature were slightly different from the primary one. These inclusions were homogenized into the vapour phase [$T_{\text{h}}(\text{LV} \rightarrow \text{V})$] at 213 to 264°C .

4.2.2 Non-aqueous inclusions (Type 2)

These inclusions are essentially carbonic-only or carbonic-rich with a thin film of aqueous liquid. The first melting temperature of these fluids occurs near the melting temperature of pure CO_2 . It seems that the carbonic inclusions ($\text{CO}_2 \pm$ other volatiles) occur in two different fluid generations. One of these inclusion generations would seem to have been developed due to the unmixing of type 1 fluid

Table 1 Microthermometric data of fluid inclusions in quartz from Kenticha rare element Pegmatites (°C)

No	Type	Size in μm	Fill (V%)	T_m (CO ₂)	T_h (CO ₂)	T_m (Cla)	T_c	T_m (ice)	T_{dms}	T_h (LV)
W8-1	AC	18	25	- 56	29.8 (l)	8.6	- 20	- 5.2	-	256 (v)
W8-2	AC	12	15	- 56	29.8 (l)	8.6	- 23	- 3	-	264 (v)
W8-3	AS	20	12	-	-	-	- 22	- 0.3	-	110 (l)
W8-4	AC	10	40	- 57	29.8 (l)	8.6	-	- 5.2	-	237 (v)
W8-5	AC	15	15	- 57.1	28.3 (l)	6	- 31	-	-	264 (v)
W8-6	AC	15	95	- 57.1	18.0 (l)	6.9	- 33	-	-	213 (v)
W8-7	AC	15	30	- 57.1	28.0 (l)	6.9	- 29	-	-	300 (v)
W8-8	AS	12	10	-	-	-	- 26	- 4.3	-	212 (l)
W8-9	AS	12	8	-	-	-	- 31	- 4.3	-	114 (l)
W8-10	AS	10	9	-	-	-	- 31	- 3.1	-	103 (l)
W-11	Ca	15	60	- 56.6	29.9 (l)	-	-	-	-	-
W9-1	AS	9	6	-	-	-	- 26	- 4.3	-	294 (l)
W9-2	AS	8	11	-	-	-	- 22	- 4.2	-	260 (l)
W9-3	AS	8	13	-	-	-	- 21	-	-	219 (l)
W9-4	AS	22	15	-	-	-	- 23	- 4.2	-	212 (l)
W9-5	AC	15	30	- 56.9	29.8 (l)	7.9	- 15	- 4.5	-	327.1 (cp)
W9-6	AC	15	45	- 56.9	29.8 (l)	7.9	- 15	- 4.5	-	327.1 (cp)
W9-7	AS	25	12	-	-	-	-	- 2.8	-	114.2 (l)
W9-8	AC	25	45	- 56.8	29.3 (l)	8.1	- 19	-	-	397.1 (cp)
W9-9	AS	26	12	-	-	-	- 18	- 5	-	265 (cp)
W9-10	AC	25	42	- 57.4	29.8 (l)	8	- 50	-	-	275 (dec)
W9-11	AC	20	30	- 56.9	28.9 (l)	8	- 4.5	-	-	376 (cp)
W9-12	AS	20	25	-	-	-	- 8.5	- 3.9	-	230 (l)
W9-13	AC + S	20	42	- 56.8	29.3 (l)	8.1	- 18	-	334	338 (l)
W9-14	AS	5	12	-	-	-	- 18	-6.5	-	239 (l)
W9-15	AC	25	42	- 56.9	29.4 (l)	8.1	-	-5.4	-	255 (dec)
W9-16	Ca	17	20	- 57.3	27.8 (l)	-	- 20	-	-	-
W9-17	Ca	17	20	- 56.8	28 (v)	-	-	-	-	-
W9-18	AC	22	24	-	29.3 (l)	8.1	- 21	-	-	275 (dec)
W14-1	AC	10	8	- 56.9	29 (l)	-	-	- 4.2	-	256 (cp)
W14-2	AS	10	9	-	-	-	- 19	- 2.9	-	129.2 (l)
W14-3	AS	12	2	-	-	-	- 22	- 5.3	-	109.2 (l)
W14-4	AS	10	12	-	-	-	-	-	-	210 (l)
W14-5	AS	14	8	-	-	-	-	- 2.9	-	129.2 (l)
W14-6	AC	18	42	- 56.9	30.1 (l)	7.9	-	-	-	288.8 (cp)
W14-7	AC	13	42	- 56.9	30.1 (l)	7.9	-	-	-	389.9 (cp)
W14-8	AS	17	10	-	-	-	-21	-5.6	-	113.5 (l)
W14-9	AC	17	40	- 56.8	29.7 (v)	7.8	-	-	-	261 (v)
W14-10	AS	8	3	-	-	-	- 21	- 5.6	-	113.5 (l)
W14-11	AC	11	60	- 56.7	28.7 (l)	8.5	-49	-	-	241.2 (cp)
W14-13	AS	7	3	-	-	-	-	- 3.7	-	160 (l)
W14-14	AC	20	42	- 56.9	30.1 (l)	7.9	-19	-	-	297 (cp)
W14-15	Ca	17	16	- 56.9	26.9 (l)	-	-	-	-	-
W14-16	AS	19	10	-	-	-	-19	-0.9	-	133 (l)
W14-17	AC	12	16	-	-	-	-19	-	-	290 (v)
W16-1	AC	10	50	- 56.9	29.8 (l)	8.2	-	-	-	314 (cp)
W-16-2	Ca	18	65	56.9	30 (v)	-	-	-	-	-
W16-3	AS	15	6	-	-	-	- 35	- 6	-	115 (l)

Table 1 continued

No	Type	Size in μm	Fill (V%)	T_m (CO ₂)	T_h (CO ₂)	T_m (Cla)	T_e	T_m (ice)	T_{dms}	T_h (LV)
W11-1	AS	14	11	–	–	–	– 31	– 8.7	–	129 (l)
W11-2	AC	18	62	57.7	28.1 (v)	7.8	–	–	–	320 (v)
W11-3	Ca	19	20	57.1	28.1 (l)	–	–	–	–	–
W11-5	Ca	20	23	– 57.1	26.4 (l)	–	–	–	–	–
W11-6	AC	18	45	– 57	30.0 (l)	7.3	–17	–	–	250 (cp)
W11-7	Ca	19	28	– 57.2	26.4 (l)	–	–	–	–	–
W11-8	AC	20	16	– 57.1	28.5 (l)	8	– 22	–	–	315 (cp)
W11-9	AC	12	42	– 57.1	28.9 (l)	8.1	–	–	–	391 (cp)
W11-10	Ca	15	35	– 57.1	27.8 (v)	–	– 25	–	–	–
W11-12	AS	23	35	–	–	–	– 22	– 4.2	–	190 (l)
W11-13	AS	20	3	–	–	–	– 24	– 8.7	–	127 (l)

No. number of measurements, AC. aqueous–carbonic, AS. aqueous–salt, Car. carbonic only, AC + S. aqueous–carbonic + solid, T_m Cla. melting temperature of clathrate, T_e . Initial temperature of ice melting, T_{dms} . temperature of dissolution of solid, T_h (LV). total homogenization temperature, l. liquid, v. vapour, cp. critical point, dec. decrepitated, As. aqueous–salt, Ca. carbonic

inclusion. This carbonic inclusion occurs coeval with the type 3 inclusions in the same crystallographic plane. Another type of carbonic-rich or carbonic-only fluid inclusion is trapped along microfracture or crystallographic planes. However, the timing of the entrapment of this inclusion is challenging to trace. This inclusion was supposedly entrapped due to the influx of fluid held within the surrounding metamorphic rocks owing to the high molar volume of the carbonic component and the presence of a nearly CO₂ phase only in the carbonic or carbonic-rich inclusions (Kerkhof and Thiéry, 2001; London, 1986; Whitworth and Rankin, 1989). It may represent fluid circulation during the latter tectonic event. The freezing point depression [$T_m(\text{CO}_2) = -56.8$ to -57.2 °C] and homogenization temperatures [$T_h(\text{CO}_2) = 26.4$ – 28.1 °C] of the carbonic inclusions are generally very close to the melting and the critical temperature of pure CO₂ system, respectively. Some of these inclusions homogenize to the vapour state [$T_h(LV \rightarrow V)$], whereas others homogenize to the liquid state via a bubble-point transition [$T_h(LV \rightarrow L)$].

4.2.3 Aqueous inclusions (Type 3)

These inclusions show wide variations in homogenization temperature (100 to 290 °C). All aqueous phase inclusions appear to be homogenized by gradual shrinkage and disappearance of the bubble phase. Type 3 inclusions are of two types, which we represent as Types 3a and 3b. Type 3a represents aqueous inclusions that form due to the unmixing of type 1 inclusions. They are relatively more saline than the parent fluid (aqueous-carbonic) and are represented by the H₂O–NaCl system. These inclusions population occur with or without filling microfracture.

These inclusions appear to be bi-phase at room temperature and show a 10–15% degree of fill. These aqueous inclusions are homogenized to a low temperature of 105 to 294 °C by the disappearance of the vapour phase. Their first ice melting temperature is near the stable eutectic temperature (T_e) of the H₂O–NaCl system, and the final ice melting temperature (T_m) ranges from -3.6 to -6.8 °C. Type 3b is abundant in low-temperature aqueous inclusions. They are secondary inclusions trapped along healed microfractures from fluid circulation during later tectonic events, probably during the uplift of the terrain. The first ice melting temperatures were well below the eutectic temperature of the H₂O–NaCl system. This might indicate the presence of additional ions such as Ca²⁺ and Mg²⁺, and the H₂O–NaCl–MgCl₂ system can represent the inclusions. The inclusions contain liquid water and a vapour phase at room temperature, with the vapour phase occupying about 6% to 15% of the total volume of the inclusions. They are irregular or oblate in shape. These fluid inclusions are secondary and trapped by the independent late-stage influx of meteoric water during or after late-stage hydrothermal activity. During cooling, the vapour bubbles shrink and eventually disappear between -23 and -35 °C, or -30 to -35 °C sensu stricto. The final melting temperature of the ices was depressed to -0.3 to -10 °C. These aqueous inclusions were homogenized into liquid via a bubble-point transition at 114 to 240 °C. This type of fluid inclusions may have been introduced during a subsolidus condition and account for the pervasive weathering of the pegmatite. The characteristics of their isochores suggest the inclusions represent the latest fluid circulation and hence postdate other inclusion types.

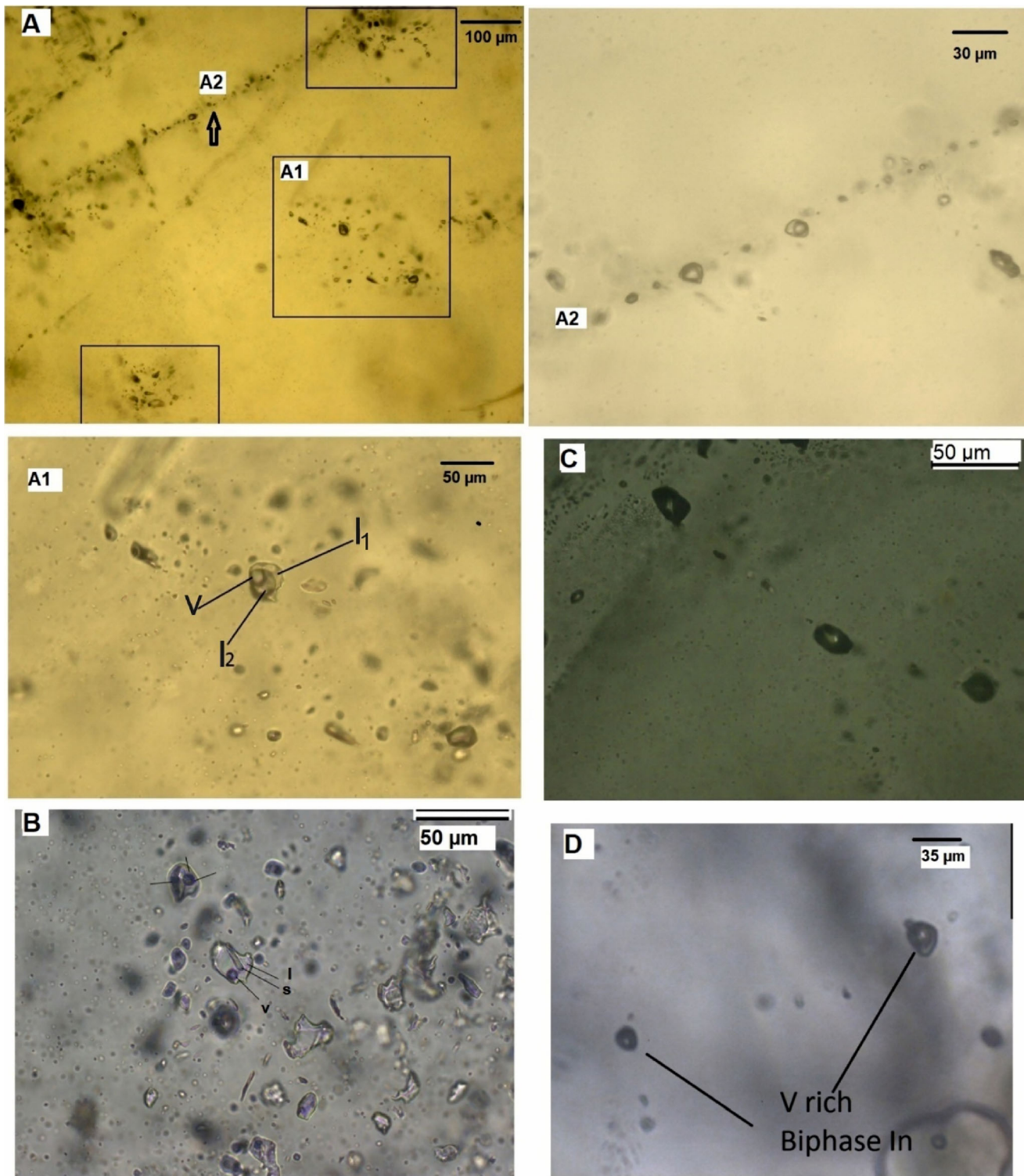


Fig. 5 Photomicrographs of fluid inclusions showing different types of inclusions: **A1.** –clusters of aqueous–carbonic inclusions, **A2.** trails of biphasic inclusions, **B.** multiphase solid inclusions with decrepitated many other inclusions, **C.** carbonic inclusions, **D.** vapour rich bi–phase inclusions in spodumene. Note that other photomicrographs are taken from quartz specimen

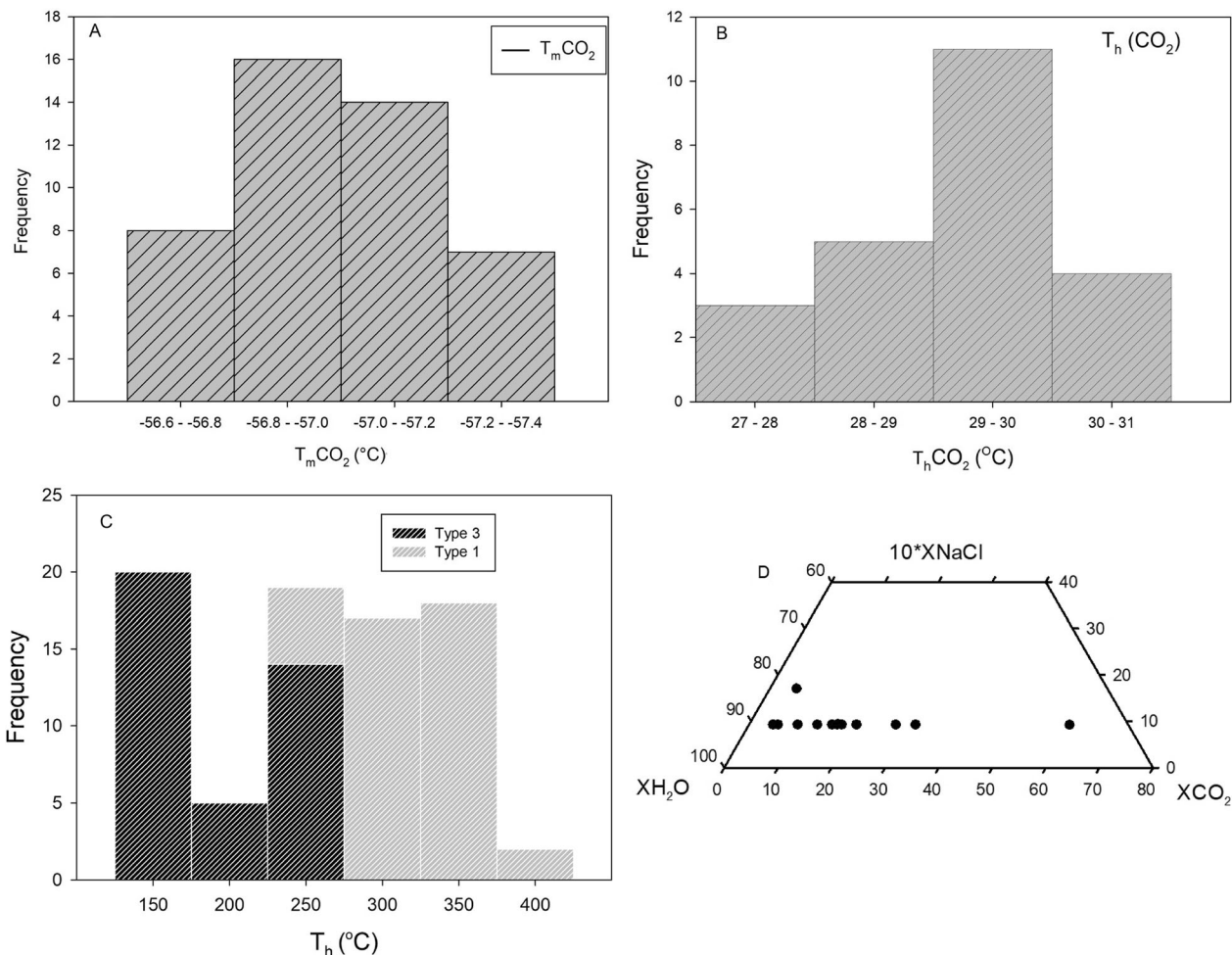


Fig. 6 Histogram of fluid inclusions data showing the frequency distribution of **A.** freezing point depression of CO_2 ($T_m\text{CO}_2$), **B.** partial homogenizations of CO_2 ($T_h\text{CO}_2$), **C.** total homogenization temperature (T_h , °C) of type-1 and type-3 inclusions, **D.** Ternary CO_2 - H_2O -10 × wt% NaCl diagram showing variation of relative proportion of H_2O - CO_2 -salt in aqueous-carbonic inclusions (type-1) from Kenticha pegmatites

4.3 Feldspar compositions

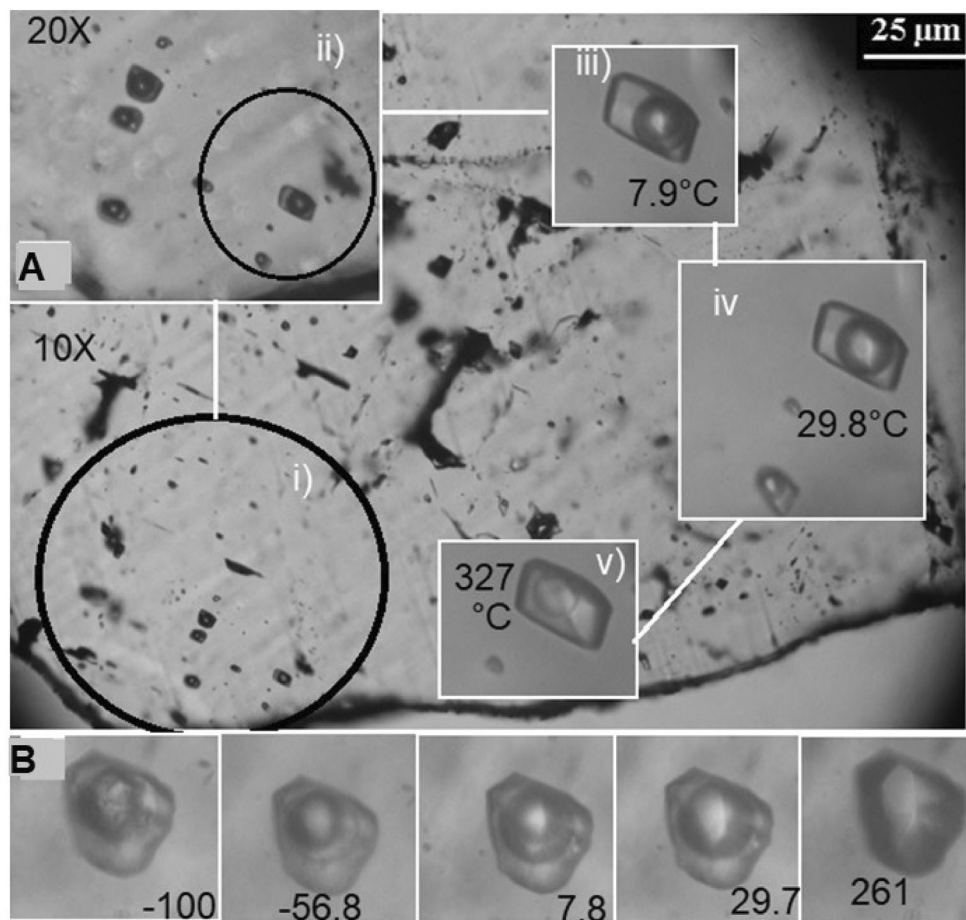
Systematic variation in feldspar composition in a different zone of the rare-metal pegmatite has been observed. The plagioclase contains 2.96–3.01 Si, 0.93–1.05 Al < 0.18 Ca, 0.80–1.02 Na and < 0.02 K in apfu. The alkali-feldspar comprises 2.90–3.09 Si, 0.92–1.11 Al; negligible Ca content (< 0.004), < 0.08 Na, and 0.88–0.96 K in apfu. Plagioclase's anorthite (An) component decreases from the wall to the core in the main Kenticha pegmatite. The overall bulk components of alkali-feldspars are $\text{Ab}_{9.4}\text{Or}_{90.3}\text{An}_{0.3}$ to $\text{Ab}_{2.2}\text{Or}_{97.6}\text{An}_{0.2}$, and the plagioclase compositions range between $\text{An}_{1.2}\text{Or}_{0.8}\text{Ab}_{98.0}$ and $\text{An}_0\text{Or}_{0.6}\text{Ab}_{99.4}$ in the rare-metal pegmatite. The anorthite (An) component of the feldspars in the aplite unit varies between 15 and 17.

5 Discussions

5.1 Fluid inclusions PTVX properties

Depending on the fluid system, appropriate equations of state have been applied to calculate the PTVX (pressure-temperature-volume-composition) relationships for each inclusion type. A C–O–H–N system containing salt solutions may represent fluid inclusions in the Kenticha pegmatite. The equation of state (EoS) given in Chen (1972), Darling (1991), and Steele-MacInnis (2018) was adopted to determine the PTVX property of type 1 inclusions whose compositions are approximated by a ternary H_2O - CO_2 -NaCl system. The compositions of the carbonic bearing inclusions were determined from the first melting of carbonic inclusions [$T_m(\text{CO}_2)$]. It was commonly homogenized just below the triple point of pure CO_2 (between -56.6 °C and -57.5 °C), which is a tell-tale sign of the presence of a very low concentration of other dissolved

Fig. 7 Photomicrographs and microthermometric data of **A.** clustered aqueous–carbonic inclusions (i and ii at 10 × and 20 × magnification respectively, iii – $T_m(\text{Cla})$, iv– $T_h\text{CO}_2$, v – total T_h , image was taken just before complete disappearances of the meniscus), **B.** decrepitation of inclusions upon progressive heating to around a temperature of around 261 °C before homogenization was achieved



gases. The salinity of aqueous-carbonic inclusions was determined from the final clathrate melting temperature [$T_m(\text{Cla})$] because the determination of salinity based on the final ice melting temperature is supposedly overestimated (Fall et al. 2011). Clathrate melting of the mixed H_2O – CO_2 inclusions has occurred in the presence of aqueous liquid, carbonic liquid and carbonic vapour phases. Therefore, a clathrate melting pressure of 35 to 43 bars was calculated from the clathrate melting temperature. Likewise, the maximum homogenization pressures of 2.6 and 3.7 kbar were calculated for inclusions homogenized to the critical phenomenon and a vapour state, respectively, using equations given in Steele-MacInnis (2018). The aqueous-carbonic inclusions have bulk densities of between 0.69 and 0.99 g/cm^3 with a corresponding molar volume of between 32.2 and 20.6 cm^3/mol . The compositions of the aqueous inclusions were determined by the first ice melting (T_i) upon heating the frozen inclusions. A computer program, AqSo_NaCl (Bakker 2018), was used to determine the aqueous-salt fluid system's isochores and other fluid P–V–T–X properties. Accordingly, a salinity of 4–12 wt% NaCl and a density of 0.8–1.0 g/cm^3 with a corresponding molar volume of 23.6–19.02 cm^3/mol were

obtained. The critical point for aqueous inclusions was determined using the software package FLUIDS, V2 (Bakker 2003), whereas the density of the non-aqueous inclusions was computed using FLUIDS, V1 (Bakker 2003). Sterner and Bodnar's (1984) EoS were used to determine the isochores of the carbonic inclusions. Those inclusions homogenized to the liquid state [$T_h(\text{LV} \rightarrow \text{L})$] have an average molar volume of 64–67 cm^3/mol with corresponding densities of 0.69–0.65 g/cm^3 . Accordingly, apart from carbon dioxide, the presence of a small amount of N_2 in the non-aqueous phase is predicted, which is estimated to be a < 0.05 mol fraction based on the Thiery et al. (1994) chart (Bekele 2020). Such inclusions were also reported in lithium pegmatites from the Bohemian Massif in the Czech Republic (Ackerman et al. 2007) and rare-element pegmatites from the Borborema province, NE Brazil (Beurlen et al. 2000). The compositions of the carbonic phase in the inclusions reflect the nature of the fluid provenance, viz., magmatic, diagenetic, metamorphic, and meteoric sources. Commonly, a binary mixture of varying proportions of H_2O and $\text{CO}_2 \pm \text{CH}_4/\text{N}_2$ is characteristic of silicic magmatic and metamorphic fluids (e.g., Ackerman et al. 2007; Lamadrid et al. 2014; Nabelek and Ternes

1997; Touret 2001; Whitworth and Rankin 1989), whereas saline brine is commonly reported as a feature of diagenetic fluids (Goldstein 2001; Wilkinson 2001).

Aqueous-carbonic inclusions are characterized by abundant gas-rich phase and homogenization phase transitions to critical phenomena [$T_h(LV) \rightarrow SCF$]. It implies that the inclusions exhibit critical specific molar volume or density, i.e., the density and composition of liquid and vapour phases close to each other. Its ternary H_2O-CO_2-NaCl plot and salinity versus homogenization temperature are given in Figs. 6D and 8, respectively. From the diagram, it is noticeable that the fluids are a fairly dilute solution. It is consistent with previous observations by Beurlen et al. (2001); London (1986); and Trumbull (1995). These and several other studies agree that primary fluids in pegmatite are characterized by relatively low to moderate salinity. However, low to moderate salinity fluid is not the rule of thumb since the presence of high salinity aqueous fluid inclusions in pegmatite has also been reported from other parts of the world (e.g., Roedder 1963).

5.2 Fluid evolution and isochores

Primary fluid may experience a sporadic compositional change during its evolution, which may be attributed to boiling, fluid-rock interactions, or meteoric water contamination. As a result, fluid inclusions trapped in either the liquid or vapour phase should be subjected to pressure correction (Roedder and Bodnar, 1980). However, for inclusions trapped along the two-phase boundary (*solvi*) and show evidence of boiling, temperature of homogenization is considered a trapping temperature, and hence

pressure correction is needless (Roedder and Bodnar 1980; Shepherd et al. 1985; Sirbescu and Nabelek 2003). Therefore, knowing fluid-phase equilibria during fluid phase formation is crucial for fluid inclusions study before interpreting microthermometric data. On this premise, the conditions of fluids during entrapment have been carefully evaluated. Evidence of boiling is indicated by the homogenization of most primary aqueous-carbonic inclusions into both liquid and vapour by the gradual fading of the meniscus. The decrease in homogenization temperature, the progressive increase in salinity, and the variable degree of fill also support boiling conditions (Canet et al. 2011; Shepherd et al. 1985). Furthermore, the presences of a cluster of aqueous-carbonic inclusions of the same generation having variable fill and the existence of an abundant gas-rich phase corroborate a condition of boiling (Canet et al. 2011). Figure 8A shows photomicrography containing fluid inclusions illustrating occurrences of coeval aqueous and non-aqueous (carbonic) inclusions accompanied by the parental, low-salinity aqueous-carbonic fluid. Therefore, the H_2O-CO_2-NaCl fluid system was a trapped primary inclusion that eventually evolved into relatively more saline aqueous inclusions and carbonic-rich or carbonic-only inclusions during the progressive evolution of the silicate melt. Boiling conditions may also be marked by the negative trend in the T_h vs. fluid salinity (Fig. 9) (Shepherd et al. (1985). It may be noted that the term “*effervescence*” is preferentially used over “*boiling*” to describe the process that produces coexisting aqueous-carbonic phases, whereas the latter term is commonly applied to a single-component system (Canet et al. 2011).

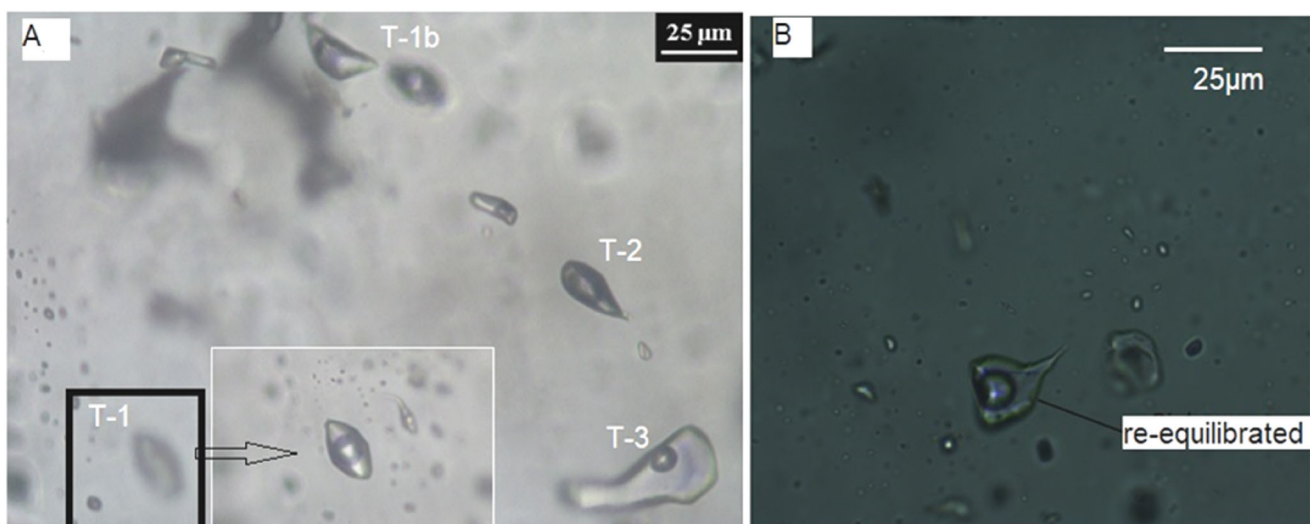


Fig. 8 Photomicrographs of fluid inclusions **A**) showing boiling and necking (T2) occurrence of carbonic and aqueous inclusions along with parental aqueous-carbonic inclusions (T refers to inclusion type) **B**) re-equilibration causing partial leakage of the large inclusions surrounded by numerous satellite inclusions

Once the fluid inclusions are entrapped and closed, the P–T path is defined by isochores. To delineate the cooling path of the rare-element pegmatite, isochores of the earliest fluid (aqueous-carbonic) inclusions were extrapolated to the thermodynamic solidus of hydrous granitic magma. The *isoplethic* P–T phase diagram of aqueous-carbonic fluid inclusions is presented on the diagram (Fig. 10A). In the figure, the high-pressure portions of the solvus curve from the present study, along with the solvus determined from experimental data by Schmidt and Bodnar (2000) for pseudobinary compositions [(H₂O + 6.0 wt.% NaCl)—21.33 mol% CO₂] were shown. The intersection of isochores of unaffected inclusions with the experimentally determined thermodynamic solidus of a haplogranite whose composition is similar to that of the Kenticha granite-pegmatite is used to approximate the P and T conditions when the initial exsolution of fluids from crystallizing silicate melt occurs. Accordingly, the fluid isochores intersect the solidus (S1) of Ebadi and Johannes (1991) at a temperature of 640–645 °C and a pressure of 2.5–3.2 kbar, whereas they intersect the solidus (S3) of Keppler (1989) between 684–685 °C and 3.0–5.1 kbar (Fig. 10B). However, the isochores would have intersected the experimentally determined solidus of melt-bearing fluxes (P₂O₅, B₂O₃, and F, 5 wt% each) presented by Veksler and Thomas (2002) to a lower P–T value.

Once the orthomagmatic fluids were exsolved and the aplite layer was crystallized, it was isobarically cooled from the petalite-spodumene phase boundary into the

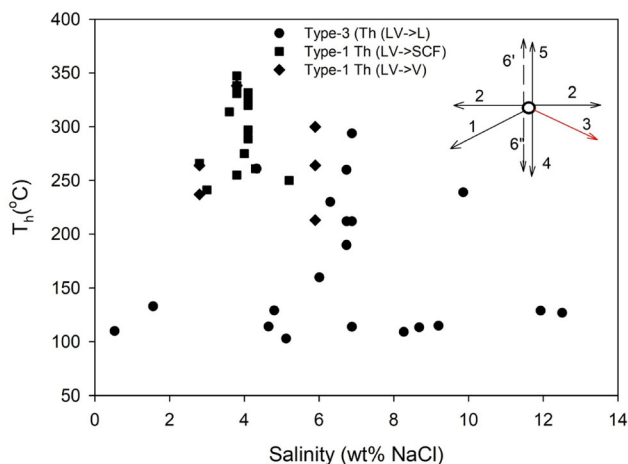


Fig. 9 A plot of salinity (wt.% NaCl) versus homogenization temperature (T_h , °C) of bulk fluid inclusions from Kenticha pegmatites, where the distribution of a large data set shows a boiling with cooling trend (trend 3). Also indicated (inset) is a general trend of various processes operating on fluid inclusions: 1. mixing with cooler and less saline fluids, 2. isothermal mixing with fluids of contrasting salinity, 3. boiling with slight cooling, 4. simple cooling, 5. leakage of inclusions during heating, 6. necking down of inclusions after Shepherd et al. (1985)

spodumene-quartz stability field until complete crystallization of the pegmatite was achieved. On the proposed pegmatite crystallization path, Fig. 10B, a drop in pressure shifts the arrow towards a lower pressure at its intersection with solvus, which is attributed to a change in lithostatic to hydrostatic pressure during fracturing. As the fluid system temperature decreases, the vapour bubble starts nucleating at the point of intersection of isochores with the solvus curve. The solvus (L–V) curve defines the limit of the two-phase liquid–vapour region (immiscibility region) at which early homogeneous fluid gets unmixed due to either T or P decrease. Inclusions trapped in one-phase field are assumed to have a similar phase ratio and homogenization temperature. From isochores-solvus intersections (Fig. 10A), it is evident that the primary aqueous-carbonic fluids start decoupling around 350 °C into carbonic-rich and more saline-aqueous inclusions. The primary aqueous-carbonic inclusions are derived from low-salinity hydrous silicate melt, whereas aqueous and non-aqueous fluid inclusions were trapped during sub-solidus conditions below 290 °C. Low salinity aqueous-carbonic inclusions with homogenization phase transition to the supercritical phenomenon, $T_h(LV \rightarrow SCF)$, are also reported in pegmatites from other parts of the world (Fuertes-fuente et al. 2000; Fuertes-Fuente and Martin-Izard 1998; Roedder 1963; Sirbescu and Nabelek 2003). According to London (1986), low-salinity late-stage magmatic or early hydrothermal fluids in pegmatites are generated due to the removal of fluxing components by tourmaline crystallization. The isochores of type 1b fluid inclusions do not intersect the experimentally determined granite solidi or may intersect the solidi at unreasonably high pressure (> 10 kbar), Fig. 10A. Presumably, this fluid represents secondary fluid inclusions trapped during post-crystallization events. The isochores of the aqueous inclusions determined using equations of state from microthermometric data are shown in Fig. 10C. The nature of the isochores of this fluid (aqueous) inclusion indicates post-crystallization hydrothermal fluid circulation.

Fluid inclusions may experience re-equilibration induced by geological processes (uplift, compression, decompression, etc.), which modify their morphologies and densities. Since re-equilibration is not uniform, unaffected, slightly modified, and completely decrepitated inclusions can occur together, even in a fluid inclusion assemblage. This phenomenon causes the P–T path of the fluid inclusions to deviate from the original isochores (Kerkhof and Hein 2001; Vityk et al. 1994). The degree of morphological modification of fluid inclusions depends on the size and composition of the inclusions and the effective pressure (the difference between lithostatic and internal pressure) (Vityk and Bodnar 1995). The effect of the pressure gradient on fluid inclusions' re-equilibration is inversely

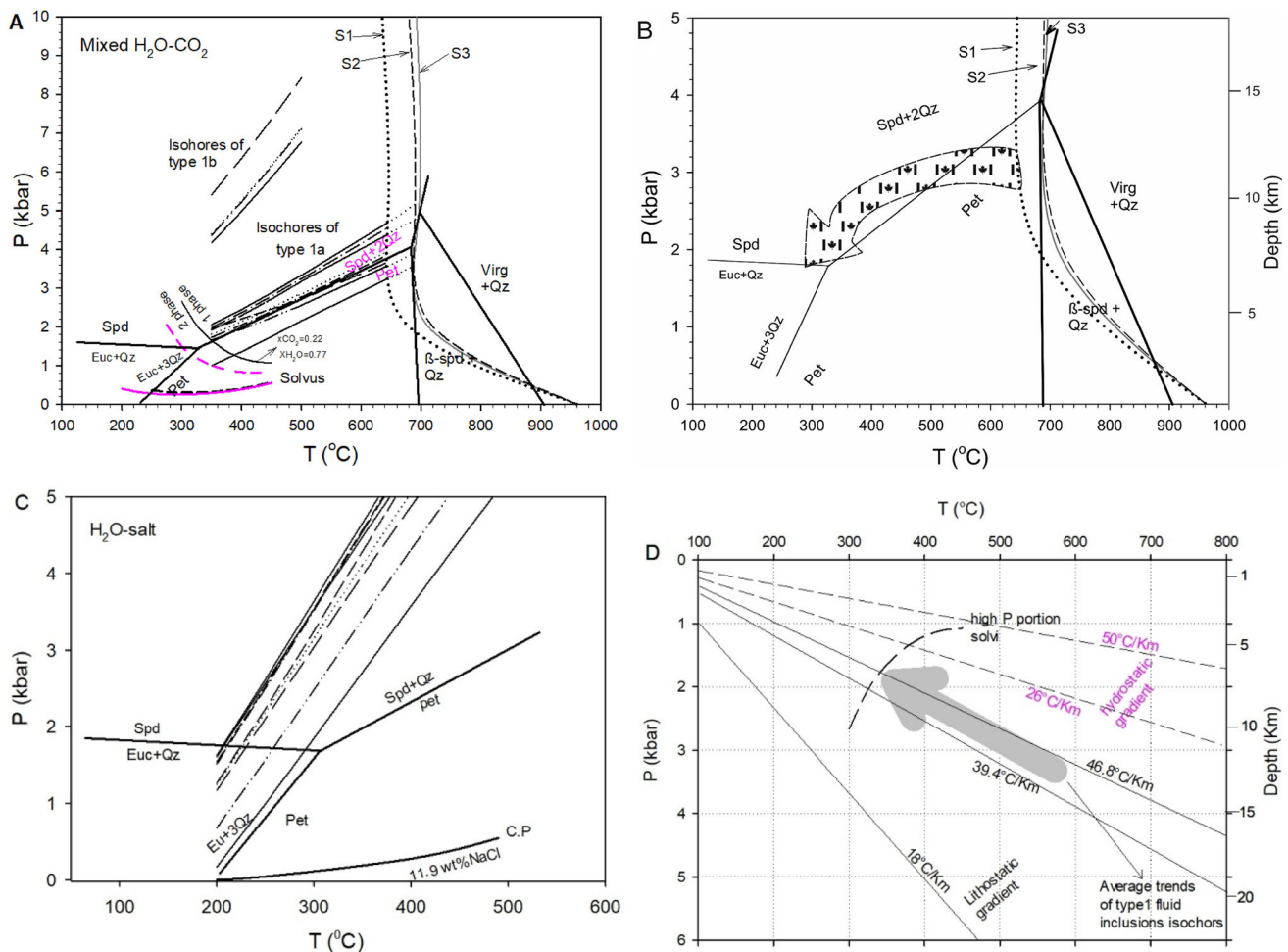


Fig. 10 **A**) P–T diagram showing isochores, low and high pressure portion *solvi* for primary aqueous–carbonic fluids and lithium–aluminosilicate stability field in the system $\text{LiAlSiO}_4\text{-SiO}_2\text{-H}_2\text{O}$ is after London (1992). Isochores are extrapolated to an experimentally determined solidus (S) of a haplogranite system determined in the presence of an $\text{H}_2\text{O-CO}_2$ fluid phase with 1.0 (S1) and 0.64 (S2) mole fraction of H_2O presented by Ebadi and Johannes (1991); and a 0.26 mol fraction of CO_2 with Na:K = 1:1 (S3) reported by Keppler (1989). A dark solid curve (solvus) is the higher pressure portion of the solvus corresponding to the composition of $\text{XCO}_2 = 0.22$ and $\text{H}_2\text{O} = 0.77$ from the present work. A pink-coloured dashed curve represents a solvus for pseudobinary compositions ($\text{H}_2\text{O} + 6.0 \text{ wt.}\% \text{ NaCl}$)–21.33 mol% CO_2 from experimental data (Schmidt and Bodnar, 2000) is included for comparisons. **B**) Schematic diagram showing the proposed P–T path for the Kenticha rare–metal granite–pegmatite with possible minor uncertainty in the curvature. The corresponding depth of emplacement is shown on the right hand side of the diagram, **C**) A P–T diagram showing isochores of aqueous ($\text{H}_2\text{O-NaCl}$) inclusions. The boiling point curve (L–V) and critical point (c.p) for a 11.9 wt% NaCl solution calculated based on Bakker (2018) for the present study is also shown in the fig. The slopes of the isochores are steep for low T_h (higher density) and flatten as T_h increases (density decreases), **D**) Schematic diagram showing an estimated geothermal gradient based on the density of H_2O and the average density of continental crust at 1 g/cm^3 and 2.7 g/cm^3 , respectively. Also shown is an average trend of primary magmatic aqueous carbonic fluid inclusions’ isochores, and high–pressure portion *solvi* with the same composition as in the previous figure. A thick grey arrow indicates the average primary magmatic fluid inclusions isochores trend, which represents the thermal gradient between the pegmatite and the country rock. Indicated thermal gradients are lithostatic (black) and hydrostatic (pink) gradients of the continental crust

proportional to the size of the fluid inclusions (Ayllón et al. 2003); i.e., large inclusions re-equilibrate at a lower effective pressure (Vityk et al. 1994). When the pressure inside the inclusion falls below the surrounding pressure (fluid under pressure) as a result of isobaric cooling or isothermal compression, the fluid inclusions re-equilibrate to the new environment through stretching, necking down, partial leakage, total decrepitation, or other methods (Canet

et al. 2011; Kerkhof and Hein 2001). In the present case, inclusions $\geq 30 \mu\text{m}$ or commonly $\geq 35 \mu\text{m}$ appear to have been affected by post-entrapment re-equilibration. It is evident from Fig. 8B that the inclusion haloes, large inclusions surrounded by satellites of inclusions, display characteristic re-equilibration under the condition of isothermal compression or isobaric cooling (Kerkhof and Hein 2001; Vallance et al. 2009). Since the Kenticha

granite-pegmatite is typically post-orogenic (Tsige 2006) and does not show any evidence of deformation, the possible effect of the isothermal compressions on re-equilibrating fluid inclusions can be ruled out. Fluid inclusions under the conditions of isothermal decompression can also cause a distinct texture. This type of inclusion re-equilibration phenomenon occurs when pressure due to overburden is lower than the fluid inclusion's internal pressure (fluid overpressure). Such a negative pressure gradient occurs in the thinned crust due to isothermal uplift and erosion (Vityk and Bodnar 1995). Therefore, in the present case, re-equilibration is likely attributed to fluid under pressure owing to isobaric cooling. Perhaps the confining pressure is below 4 kbar, as discussed in the next section. Such a phenomenon commonly occurs during the last stage of the orogenic process. Re-equilibrations are evident from textural features shown both in primary and secondary inclusions. As a result, the nature of re-equilibrated fluid inclusion morphology is not only a measure of how the P–T path of the fluid inclusions deviates from the actual isochoric path, but it is also a viable indicator of the host rock's tectonic evolution (Kerkhof and Hein 2001; Vityk et al. 1994). However, detailed treatment of re-equilibration criteria to infer tectonic evolution is beyond the scope of this paper. Hence, the reader is referred to Kerkhof and Hein (2001) and Vityk and Bodnar (1995) for better information.

5.3 Crystallization conditions of the rare element pegmatite

The final crystallization history of the Kenticha rare element pegmatite was reconstructed by integrating the microthermometric and two-feldspar geothermometric data. According to the microthermometric observation, the fluids (H₂O–CO₂–NaCl system) were entrapped at a minimum temperature of 397 °C and a lithostatic pressure of ≈ 2 kbar from the boiling fluids during the final stage of the rare-element pegmatite crystallization. An independent estimate of the temperature of the main-stage crystallization condition based on the two-feldspar geothermometer has also been carried out to determine the trapping temperature (T_t). The assumption is that the compositions of coexisting feldspar pairs are dictated solely by the pressure and temperature conditions provided that the two feldspars attain complete stable equilibrium (Benisek et al. 2004; Elkins and Grove 1990; Green and Usdansky 1986; Jiao and Guo 2011). Moreover, the model of albite distribution between plagioclase and alkali feldspar requires that the confining pressure at the time of equilibration be estimated. A pressure of one to two kbar was estimated since the pegmatites were intruded into an epizonal environment (i.e., greenschist facies country rocks), which is thought to

have been only a few kilometres deep. Understandably, if the pegmatites were intruded into a higher P–T condition, the immiscible liquid would not have occurred as primary inclusions. Furthermore, the presence of spessartine-rich garnet in the Kenticha pegmatite has been revealed by our recent study (Bekele and Sen 2020), which is assumed to have been emplaced at a pressure below 5 kbar or down to below 1 kbar (Manning 1983). The presence of primary petalite (see lithium aluminosilicate phase reaction relationship) also supports the emplacement of the rare-metal pegmatite at low pressure (3.5 kbar). The equilibrium temperature for the Kenticha rare-element pegmatite and associated granite was calculated at a pressure of 1 & 2 kbar using the Margules model of Benisek et al. (2004) with the help of the SolvCalc2 program developed by Wen and Nekvasil (1994) from appropriate coexisting feldspar pairs. Accordingly, an equilibration temperature range between 405 and 435 °C was obtained for the Kenticha rare-element granite-pegmatite, assuming a maximum confining pressure of 2 kbar (Table 2). At a pressure of 2 kbar, a slight decrease in temperature from the lower to the upper zone was observed. A temperature of about 449 °C and 573 °C were obtained for the barren pegmatite and the “parental” two-mica granite pluton (Kilta Shambali), respectively. Crystallization temperatures obtained using the determinative curve (Stormer 1975) show a fair agreement with the available ternary feldspar geothermometer (Fig. 11). Such a low crystallization temperature has been reported for pegmatites from other parts of the world. For example, based on oxygen isotope equilibrium temperatures between quartz and coexisting feldspar, Nabelek et al. (1992) have determined a temperature down to 350 °C from Harney Peak Granite and associated rare-element pegmatite in the Black Hills, South Dakota. Similarly, based on fluid inclusions studies, Sirbescu and Nabelek (2003) have reported a temperature of 340 °C for Li-bearing Tin Mountain pegmatite, Black Hills, South Dakota. However, the result of the present study is slightly below the experimentally determined solidus temperature of 450–500 °C, which was reported by Veksler and Thomas (2002) from flux-rich (B, P, and F) synthetic granitic pegmatite at a pressure of 1 and 2 kbar. Likewise, to break down petalite to spodumene in the Tanco Pegmatite, London (1982) pointed out that a temperature of 455–475 °C and a pressure of 2.4–2.9 kbar were required. The absence of notable fluid inclusions in the aplitic layer of the Kenticha rare element granite-pegmatite may suggest slow cooling in the parent magma chamber promotes fluid inclusions partitioning the remaining melt. According to Nabelek et al. (2010) and references therein, the occurrences of pegmatites are unlikely to occur from slow cooling magmas devoid of fluid/volatile components. Thus, we can assume that the presence of volatiles and fluxing

Table 2 The equilibrium temperature calculated using the Margules model of Benisek et al. (2004) with the help of the SolvCalc2 program developed by Wen and Nekvasil (1994) for Kenticha pegmatites and associated granite at a pressure of 1 & 2 kbar for suitable co-existing feldspar pairs

Sample	Plagioclase feldspar			Alkali feldspar			1kbar T (°C)	2 kbar T (°C)	Sample source
	Ab	Or	An	Ab	Or	An			
KS	80.2	1.81	18	11.2	88.5	0.2	568.4	572.9	KS granite
K-S-6	99.1	0.46	0.42	7.04	92.9	0.1	446.8	448.8	Barren pegmatite
K151	6.35	93.6	0.03	6.56	93.4	0	500	505	Aplitic granite
K112	99.4	0.6	0.05	7.13	92.8	0.1	429	430.9	IZ RM pegmatite
K109	98.6	1.19	0.22	7.45	92.5	0	410	411.8	CZ RM pegmatite

IZ intermediate zone, CZ core zone, RM rare metal

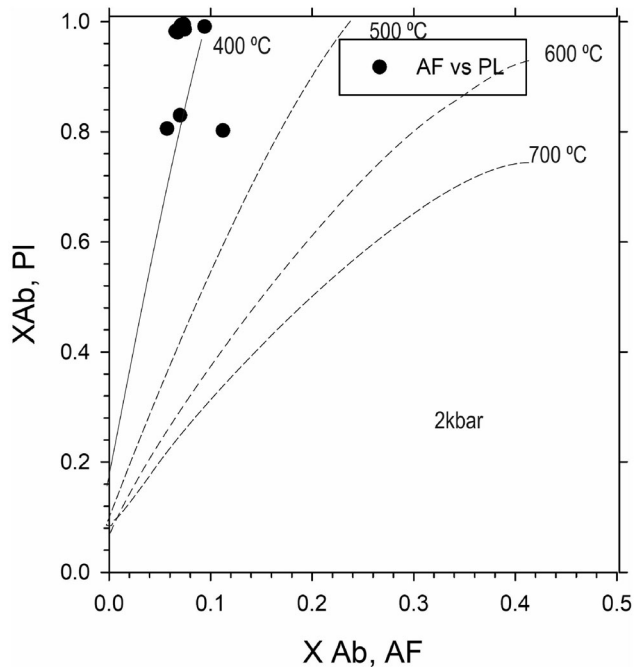


Fig. 11 A plot of albite distribution between coexisting feldspars, equilibrium temperature calibration curves after Stormer Jr (1975)

components in the melt could depress the liquidus sufficiently and cause the intersection of the subsolidus-solvus surface at a low temperature (e.g., Nabelek et al. 2010). As a result, the remaining melt gets undercooled to form the rare-element pegmatite under non-equilibrium crystallization.

The determined temperature–pressure conditions may point out the thermal history of the Kenticha area in the Neoproterozoic. As mentioned above, the projection of isochore into the experimentally determined volatile bearing haplogranite solidus indicates the exsolution of the fluids from the silicate melt around a temperature of 643 °C and 2.7 kbar pressure at the upper petalite-spodumene boundary in the lithium aluminosilicate phase diagram. Its corresponding depth of emplacement is around 11 km, as shown on the right-hand side of Fig. 10D. This indicates the emplacement of the parental magma at the upper crustal depths, according to the crustal structure

presented in Rudnick and Gao (2013). The depth is proportional to about 40–46 °C/km of geothermal gradients (Fig. 10D), assuming a fluid density of 1 g/cm³ and an average density of 2.7 g/cm³ for the overlying rock mass. A slightly higher depth of regional metamorphism (hence geothermal gradient) was constrained for semi-pelitic country rocks of the Kenticha area using an equilibrium garnet-plagioclase-biotite geothermometer (Yihunie et al. 2004).

6 Conclusions

Fluid inclusions representing episodic fluid circulations were entrapped during and post-pegmatite crystallization. Microthermometric studies reveal three major fluid inclusion types in Kenticha pegmatites: aqueous-carbonic, aqueous, and non-aqueous phase inclusions. The primary aqueous-carbonic inclusion is possibly a late-magmatic or early hydrothermal fluid that is closely related to the occurrence of the highly evolved Kenticha rare-element pegmatite. The entrapment of the post-crystallization fluid of metamorphic origin is proved by the presence of a nearly pure CO₂ phase in the carbonic or carbonic-rich inclusions. The latest fluid inclusions were entrapped by post-solidification hydrothermal circulation that accounts for the pervasive alteration in the aplite and pegmatite units. The earliest fluid entrapped was low-salinity aqueous-carbonic fluids approximated by an H₂O-CO₂-NaCl system. This fluid is assumed to have been exsolved from the evolved hydrous silicate melt and eventually unmixed into the coeval pure CO₂ and H₂O-salt system during uplift or the Kenticha pegmatite solidification. The primary fluid was trapped under the conditions of boiling and subsequently cooled isobarically until the final crystallization stage of the pegmatite melt. The P–T crystallization conditions determined using a two-feldspar geothermometer are consistent with fluid inclusion microthermometry. Accordingly, a final crystallization temperature between 397 °C (min. crystallization T based on fluid inclusion) and 435 °C (max. crystallization T based on feldspar geothermometer)

was estimated for the Kenticha rare-element pegmatite, assuming a maximum confining pressure of 2 kbar. Such a large undercooling is attributed to the activity of hyperfusible components, which enhance crystal growth but decrease the nucleation rate. A slight decrease in temperature from the basal granitic lower zone to the upper zone of pegmatite was observed, which is consistent with the crystallization trend of a zoned pegmatite.

Acknowledgements The authors are grateful to Dr. R. Krishnamurthi, Department of Earth Sciences, IIT Roorkee, India for permitting them access to the microthermometry facilities. We thank Mr. Kamlesh Kumar Meena for assisting during the Microthermometry lab work. The support provided by the Ethiopian Mineral, Petroleum and Biofuel Corporation (EMPBC) during the fieldwork deserves special gratitude. Mr. Mathios G/Wold from EMPBC is thankful for his support during the fieldwork.

Funding The author received no funding from external sources.

Declaration

Conflict of interest The authors declare that they have no known competing financial interests or personal relationships that could have appeared to influence the work reported in this paper.

References

- Ackerman L, Zachariáš J, Pudilová M (2007) P-T and fluid evolution of barren and lithium pegmatites from Vlastějovice, Bohemian Massif, Czech Republic. *Int J Earth Sci* 96:623–638. <https://doi.org/10.1007/s00531-006-0133-3>
- Allen A, Tadesse G (2003) Geological setting and tectonic subdivision of the Neoproterozoic orogenic belt of Tuludimtu, western Ethiopia. *J Afr Earth Sci* 36:329–343. [https://doi.org/10.1016/S0899-5362\(03\)00045-9](https://doi.org/10.1016/S0899-5362(03)00045-9)
- Anderson AJ, Clark AH, Gray S (2001) The occurrence and origin of zabuyelite (Li₂CO₃) in spodumene-hosted fluid inclusions: implications for the internal evolution of rare-element granitic pegmatites. *Can Miner* 39:1513–1527
- Ayllón F, Bakker RJ, Warr LN (2003) Re-equilibration of fluid inclusions in diagenetic-anchizonal rocks of the Ciñera-Matalana coal basin (NW Spain). *Geofluids* 3:49–68. <https://doi.org/10.1046/j.1468-8123.2003.00048.x>
- Bakker RJ (2003) Package FLUIDS 1. Computer programs for analysis of fluid inclusion data and for modelling bulk fluid properties. *Chem Geol* 194:3–23
- Bakker RJ (2018) AqSo_NaCl: computer program to calculate p-T-V-x properties in the H₂O-NaCl fluid system applied to fluid inclusion research and pore fluid calculation. *Comput Geosci* 115:122–133. <https://doi.org/10.1016/j.cageo.2018.03.003>
- Bakker RJ, Diamond L (2006) Estimation of volume fractions of liquid and vapor phases in fluid inclusions, and definition of inclusion shapes. *Am Miner* 91:635–657
- Bekele B (2020) Genesis and Evolution of Kenticha Rare-Element Granite-Pegmatite, Southern Ethiopia. PhD Thesis. Indian Institute of Technology Roorkee, Roorkee, India.
- Bekele B, Sen AK (2020) The mineral chemistry of gahnite, garnet and columbite-group minerals (CGM): implications for genesis and evolution of the Kenticha Rare-element granite-pegmatite, Adola, Ethiopia. *J Afr Earth Sci* 162:103691. <https://doi.org/10.1016/j.jafrearsci.2019.103691>
- Benisek A, Kroll H, Cemic L (2004) New developments in two-feldspar thermometry. *Am Miner* 89:1496–1504
- Beraki WH, Bonavia F, Getachew T, Schmerold R, Tarekegn T (1989) The Adola Fold and Thrust Belt, southern Ethiopia: a re-examination with implications for Pan-African evolution. *Geol Mag* 126(06):647–657. <https://doi.org/10.1017/S0016756800006944>
- Beurlen H, Da Silva MRR, De De Castro C (2000) Fluid origin and evolution during the formation of rare-element pegmatites from the borborema province. *Northeast Brazil Rev Bras Geociências* 30:331–336
- Beurlen H, Da Silva MRR, De Castro C (2001) Fluid inclusion microthermometry in Be-Ta-(Li-Sn)-bearing pegmatites from the Borborema Province, Northeast Brazil. *Chem Geol* 173:107–123. [https://doi.org/10.1016/S0009-2541\(00\)00270-9](https://doi.org/10.1016/S0009-2541(00)00270-9)
- Bisrat Y, Reimold WU, Armstrong R, Koeberl C, Anhaeusser CR, Phillips D (2002) The tectonostratigraphy, granitoid geochronology and geological evolution of the Precambrian of southern Ethiopia. *J Afr Earth Sci* 34:57–84
- Bisrat Y, Reimold WU, Anhaeusser CR, Koeberl C (2003) Geochemistry of the mafic rocks of the ophiolitic fold and thrust belts of southern Ethiopia: constraints on the tectonic regime during the Neoproterozoic (900–700 Ma). *Precambrian Res* 121:157–183
- Brown WL, Parsons I (1981) Towards a more practical two-feldspar geothermometer. *Contrib Miner Pet* 76:369–377
- Cameron EN, Rowe RB, Weis PL (1953) Fluid inclusions in Beryl and Quartz from Pegmatites of the Middletown District, Connecticut. *Am Miner J Earth Planet Mater* 38(3–4):218–262
- Canet C, Franco SI, Prol-Ledesma RM, González-Partida E, Villanueva-Estrada RE, Prol-Ledesma RM, González-Partida E, Villanueva-Estrada RE (2011) A model of boiling for fluid inclusion studies: application to the Bolaños Ag-Au-Pb-Zn epithermal deposit, Western Mexico. *J Geochem Explor* 110(2):118–125. <https://doi.org/10.1016/j.gexplo.2011.04.005>
- Černý P (1991) Rare-element granitic pegmatites. Part I: anatomy and internal evolution of pegmatite deposits. *Geosci Can* 18(2):49–67
- Chen HS (1972) The thermodynamics and composition of carbon dioxide hydrate. Syracuse University, Syracuse, New York
- Darling RS (1991) An extended equation to calculate NaCl contents from final clathrate melting temperatures in H₂O-CO₂-NaCl fluid inclusions: implications for P-T isochore location. *Geochim Cosmochim Acta* 55(12):3869–3871
- Diamond LW (2003) Glossary: terms and symbols used in fluid inclusion studies. *Fluid Incl Anal Interpret* 32:363–372
- Ebadi A, Johannes W (1991) Beginning of melting and composition of first melts in the system Qz-Ab-Or-H₂O-CO₂. *Contrib Miner Petrol* 106:286–295
- Elkins LT, Grove TL (1990) Ternary feldspar experiments and thermodynamic models. *Am Miner* 75:544–559
- Fall A, Tattitch B, Bodnar RJ (2011) Combined microthermometric and Raman spectroscopic technique to determine the salinity of H₂O-CO₂-NaCl fluid inclusions based on clathrate melting. *Geochim Cosmochim Acta* 75:951–964. <https://doi.org/10.1016/j.gca.2010.11.021>
- Fritz H, Abdelsalam M, Ali KA, Bingen B, Collins AS, Fowler AR, Ghebreab W, Hauzenberger CA, Johnson PR, Kusky TM, Macey P, Muhongo S, Stern RJ, Viola G (2013) Orogen styles in the East African Orogen: a review of the Neoproterozoic to Cambrian tectonic evolution. *J Afr Earth Sci* 86:65–106. <https://doi.org/10.1016/j.jafrearsci.2013.06.004>

- Fuertes-fuente M, Martin-izard A, Boiron MC, Viñuela JM (2000) P-T Path and fluid evolution in the Franqueira granitic pegmatite, central Galicia, Northwestern Spain. *Can Miner* 38:1163–1175
- Fuertes-Fuente M, Martin-Izard A (1998) The Forcarei Sur rare-element granitic pegmatite field and associated mineralization, Galicia, Spain. *Can Miner* 36:303–325
- Goldstein RH (2001) Fluid inclusions in sedimentary and diagenetic systems. *Lithos* 55:159–193
- Goldstein RH, Reynolds T (1994) Systematics of fluid inclusions in diagenetic minerals. *SEPM Short Course* 31:199
- Green NL, Usdansky SI (1986) Ternary-feldspar mixing relations and thermobarometry. *Am Miner* 71(9–10):1100–1108. <https://doi.org/10.1007/BF00307762>
- Hailu W, Schandelmeier H (1996) Tectonic evolution of the Neoproterozoic Adola Belt of southern Ethiopia: evidence for a Wilson Cycle process and implications for oblique plate collision. *Precambrian Res* 77:179–210. [https://doi.org/10.1016/0301-9268\(95\)00054-2](https://doi.org/10.1016/0301-9268(95)00054-2)
- Jahns RH, Burnham CW (1969) Experimental studies of pegmatite genesis: I, a model for the derivation and crystallization of granitic pegmatites. *Econ Geol* 68:843–864
- Jiao S, Guo J (2011) Application of the two-feldspar geothermometer to ultrahigh-temperature (UHT) rocks in the Khondalite belt, North China craton and its implications. *Am Miner* 96:250–260. <https://doi.org/10.2138/am.2011.3500>
- Kepler H (1989) The influence of the fluid phase composition on the solidus temperatures in the haplogranite system $\text{NaAlSi}_3\text{O}_8$ - KAlSi_3O_8 - SiO_2 - H_2O - CO_2 . *Contrib Miner Petrol* 102:321–327
- Küster D (2009) Granitoid-hosted Ta mineralization in the Arabian-Nubian Shield: ore deposit types, tectono-metallogenetic setting and petrogenetic framework. *Ore Geol Rev* 35:68–86. <https://doi.org/10.1016/j.oregeorev.2008.09.008>
- Küster D, Romer RL, Tolessa D, Zerihun D, Bheemalingeswara K, Melcher F, Oberthür T (2009) The Kenticha rare-element pegmatite, Ethiopia: internal differentiation, U-Pb age and Ta mineralization. *Miner Depos* 44:723–750. <https://doi.org/10.1007/s00126-009-0240-8>
- Lamadrid HM, Lamb WM, Santosh M, Bodnar RJ (2014) Raman spectroscopic characterization of H_2O in CO_2 -rich fluid inclusions in granulite facies metamorphic rocks. *Gondwana Res* 26:301–310. <https://doi.org/10.1016/j.gr.2013.07.003>
- London D (1986) Magmatic-hydrothermal transition in the Tanco rare-element pegmatite: evidence from fluid inclusions and phase-equilibrium experiments. *Am Miner* 71:376–395
- London D (1992) The Application of experimental petrology to the genesis and crystallization of granitic pegmatites. *Can Miner* 30:499–540
- London D, Kontak DJ (2012) Granitic pegmatites: scientific wonders and economic bonanzas. *Elements* 8:257–261. <https://doi.org/10.2113/gselements.8.4.257>
- London D, Morgan GB (2012) The pegmatite puzzle. *Elements* 8:263–268. <https://doi.org/10.2113/gselements.8.4.263>
- London D, Spooner ETC, Roedder E (1982) Fluid-solid inclusions in spodumene from the Tanco pegmatite, Bernic Lake, Manitoba. *Carnegie Inst Washingt Year b* 81:334–339
- Manning DAC (1983) Chemical variation in garnets from aplites and pegmatites, peninsular Thailand. *Miner Mag* 47:353–358
- Nabelek PI, Ternes K (1997) Fluid inclusions in the Harney Peak Granite, Black Hills, South Dakota, USA: implications for solubility and evolution of magmatic volatiles and crystallization of leucogranite magmas. *Geochim Cosmochim Acta* 61:1447–1465. [https://doi.org/10.1016/S0016-7037\(97\)00006-9](https://doi.org/10.1016/S0016-7037(97)00006-9)
- Nabelek PI, Russ-Nabelek C, Denison JR (1992) The generation and crystallization conditions of the Proterozoic Harney Peak Leucogranite, Black Hills, South Dakota, USA: petrologic and geochemical constraints. *Contrib Miner Petrol* 110:173–191. <https://doi.org/10.1007/BF00310737>
- Nabelek PI, Whittington AG, Sirbescu MLC (2010) The role of H_2O in rapid emplacement and crystallization of granite pegmatites: resolving the paradox of large crystals in highly undercooled melts. *Contrib Miner Petrol* 160:313–325. <https://doi.org/10.1007/s00410-009-0479-1>
- Pouchou JL, Pichoir F (1991) Quantitative analysis of homogeneous or stratified microvolumes applying the model “PAP.” In: Heinrich KFJ, Newbury DE (eds) *Electron probe quantitation*. Springer, Boston, MA
- Roedder E (1963) Studies of fluid inclusions II: freezing data and their interpretation. *Econ Geol* 58(2):167–208
- Roedder E (1981) Origin of fluid inclusion and changes that occur after trapping. In: Hollister LS, Crawford ML (eds) *Short course handbook-fluid inclusion: application to petrology*. Mineralogical Association of Canada, Reston, USA
- Roedder E (1984) Fluid inclusions, reviews in mineralogy. *Miner Soc Am* 12:646
- Roedder E, Bodnar RJ (1980) Geologic pressure determinations from fluid inclusion studies. *Annu Rev Earth Planet Sci* 8:263–301
- Rudnick RL, Gao S (2003) Composition of the continental crust. *Treatise Geochem* 3:1–64
- Schmidt C, Bodnar RJ (2000) Synthetic fluid inclusions: XVI. PVTX properties in the system H_2O - NaCl - CO_2 at elevated temperatures, pressures, and salinities. *Geochim Cosmochim Acta* 64:3853–3869. [https://doi.org/10.1016/S0016-7037\(00\)00471-3](https://doi.org/10.1016/S0016-7037(00)00471-3)
- Shelton KL, Orville PM (1980) Formation of synthetic fluid inclusions in natural quartz. *Am Miner* 65:1233–1236
- Shepherd TJ, Ranbin AH, Alderton DHM, (1985) *A practical guide to fluid inclusion studies*. Glasgow and London (Blackie). Mineralogical magazine, London.
- Sirbescu M-LC, Nabelek PI (2003) Crystallization conditions and evolution of magmatic fluids in the Harney Peak Granite and associated pegmatites, Black Hills, South Dakota — evidence from fluid inclusions. *Geochim Cosmochim Acta* 67:2443–2465. [https://doi.org/10.1016/S0016-7037\(02\)01408-4](https://doi.org/10.1016/S0016-7037(02)01408-4)
- Solomon T, Zerihun D (1996) Composition, fractional trend and zoning accretion of the columbite-tantalite group of mineral in the Kenticha rare-metal field (Adola, Southern Ethiopia). *J Afr Earth Sci* 23:411–431
- Solomon T, Zerihun D (1996) Composition, fractionation trend and zoning accretion of the columbite-tantalite group of minerals in the Kenticha rare-metal field (Adola, southern Ethiopia). *J Afr Earth Sci* 23:411–431. [https://doi.org/10.1016/S0899-5362\(97\)00010-9](https://doi.org/10.1016/S0899-5362(97)00010-9)
- Steele-MacInnis M (2018) Fluid inclusions in the system H_2O - NaCl - CO_2 : an algorithm to determine composition, density and isochore. *Chem Geol* 498:31–44. <https://doi.org/10.1016/j.chemgeo.2018.08.022>
- Stern RJ, Dawoud AS (1991) Late precambrian (740 Ma), charnokite, enderbite, and granite from Jebel Moya, Sudan: a link between the Mozambique Belt and the Arabian-Nubian Shield. *J Geol* 99:648–659
- Stern RJ, Ali KA, Abdelsalam MG, Wilde SA, Zhou Q (2012) U-Pb zircon geochronology of the eastern part of the Southern Ethiopian Shield. *Precambrian Res* 206–207:159–167. <https://doi.org/10.1016/j.precamres.2012.02.008>
- Stern SM, Bodnar RJ (1984) Synthetic fluid inclusions in natural quartz I. Compositional types synthesized and applications to experimental geochemistry. *Geochim Cosmochim Acta* 48:2659–2668
- Storner JCJ (1975) A practical two-feldspar geothermometer. *Am Miner* 60:667–674
- Tadesse S (2001) Geochemistry of the pegmatitic rocks and minerals in the Kenticha Belt, Southern Ethiopia: implication to

- geological setting. *Gondwana Res* 4:97–104. [https://doi.org/10.1016/S1342-937X\(05\)70658-4](https://doi.org/10.1016/S1342-937X(05)70658-4)
- Tadesse Y, Adachi M, Takeuchi M (2004) P-T conditions of metamorphism in the Neoproterozoic rocks of the Negele area, Southern Ethiopia. *Gondwana Res* 7:489–500. [https://doi.org/10.1016/S1342-937X\(05\)70800-5](https://doi.org/10.1016/S1342-937X(05)70800-5)
- Thiery R, van den Kerkhof AM, Dubessy J (1994) VX properties of CO₂-CH₄ and CO₂-N₂ fluid inclusions: modelling for T < 31°C and P < 400 bars. *Eur J Miner* 6:753–771
- Touret JLR (2001) Fluids in metamorphic rocks. *Lithos* 55:1–25
- Trumbull RB (1995) Mineralogy petrology a fluid inclusion study of the Sinceni rare-element pegmatites of Swaziland. *Miner Petrol* 55:85–102
- Tsige L (2006) Metamorphism and gold mineralization of the Kenticha-Katawicha area: Adola belt, southern Ethiopia. *J African Earth Sci* 45:16–32. <https://doi.org/10.1016/j.jafrearsci.2006.01.002>
- Vallance J, Fontboté L, Chiaradia M, Markowski A, Schmidt S, Vennemann T (2009) Magmatic-dominated fluid evolution in the Jurassic Nambija gold skarn deposits (southeastern Ecuador). *Miner Depos* 44(4):389–413. <https://doi.org/10.1007/s00126-009-0238-2>
- van den Kerkhof AM, Hein UF (2001) Fluid inclusion petrography. *Lithos* 55:27–47
- van den Kerkhof AM, Thiéry R (2001) Carbonic inclusions. *Lithos* 55:49–68
- Veksler IV, Thomas R (2002) An experimental study of B-, P- and F-rich synthetic granite pegmatite at 0.1 and 0.2 GPa. *Contrib Miner Petrol* 143:673–683. <https://doi.org/10.1007/s00410-002-0368-3>
- Vityk MO, Bodnar RJ (1995) Textural evolution of synthetic fluid inclusions in quartz during reequilibration, with applications to tectonic reconstruction. *Contrib Miner Petrol* 121:309–323. <https://doi.org/10.1007/BF02688246>
- Vityk MO, Bodnar RJ, Schmidth CS, Schmidt CS (1994) Fluid inclusions as tectonothermobarometers: relation between pressure-temperature history and reequilibration morphology during crustal thickening. *Geology* 22:731–734
- Wen S, Nekvasil H (1994) SOLVCALC: an interactive graphics program package for calculating ternary feldspar solvus and two-feldspar geothermometry. *Comput Geosci* 20:1025–1040
- Whitworth MP, Rankin AH (1989) Evolution of fluid phases associated with lithium pegmatites from SE Ireland. *Mineral Mag* 53:271–284
- Wilkinson JJ (2001) Fluid inclusions in hydrothermal ore deposits. *Lithos* 55:229–272
- Wood SA, Williams-jones AE (1993) Theoretical studies of the alteration of spodumene, petalite, eucryptite and pollucite in granitic pegmatites: exchange reactions with alkali feldspars. *Contrib Miner Pet*. <https://doi.org/10.1007/BF00307760>
- Yihunie T, Adachi M, Takeuchi M (2004) P-T Conditions of Metamorphism in the Neoproterozoic Rocks of the Negele Area Southern Ethiopia. *Gondwana Res* 7(2):489–500. [https://doi.org/10.1016/S1342-937X\(05\)70800-5](https://doi.org/10.1016/S1342-937X(05)70800-5)
- Zerihun D, Garbarino C, Valera R (1995) Granite pegmatite system in Kenticha (Adola, Sidamo, Ethiopia) rare-metal pegmatite belt: petrochemistry regional pegmatite zoning and classification. *SENET Ethiop J Sci* 18:119–148